2010

Rocket motor segmenting

Jeffrey Lynn Lee

ROCKET MOTOR SEGMENTING

by

JEFFREY LYNN LEE

A THESIS

Submitted in partial fulfillment of the requirements
for the degree of Master of Science in Engineering
in
The Department of Mechanical and Aerospace Engineering
to
The School of Graduate Studies
of
The University of Alabama in Huntsville

HUNTSVILLE, ALABAMA

2010

In presenting this thesis in partial fulfillment of the requirements for a master's degree from The University of Alabama in Huntsville, I agree that the Library of this University shall make it freely available for inspection. I further agree that permission for extensive copying for scholarly purposes may be granted by my advisor or, in his absence, by the Chair of the Department or the Dean of the School of Graduate Studies. It is also understood that due recognition shall be given to me and to the University of Alabama in Huntsville in any scholarly use which may be made of any material in this thesis.

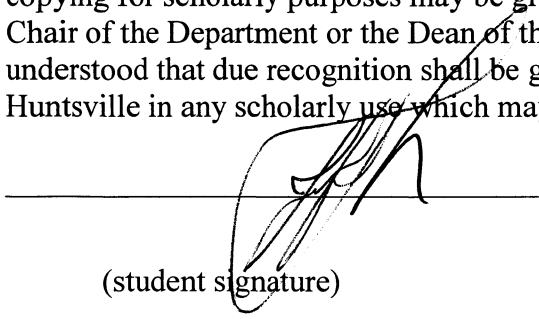

2/24/10

(student signature) (date)

THESIS APPROVAL FORM

Submitted by Jeffrey Lee in partial fulfillment of the requirements for the degree of Master of Science in Engineering in Mechanical and Aerospace Engineering and accepted on behalf of the Faculty of the School of Graduate Studies by the thesis committee.

We, the undersigned members of the Graduate Faculty of The University of Alabama in Huntsville, certify that we have advised and/or supervised the candidate on the work described in this thesis. We further certify that we have reviewed the thesis manuscript and approve it in partial fulfillment of the requirements for the degree of Master of Science in Engineering in Mechanical and Aerospace Engineering.

2/24/10 Committee Chair

(Date)

2/24/10

2-24-10

3/3/10 Department Chair

3/8/10 College Dean

4/21/10 Graduate Dean

ABSTRACT
The School of Graduate Studies
The University of Alabama in Huntsville

Degree Master of Science in Engineering College/Dept. Engineering/Mechanical and Aerospace Engineering

Name of Candidate Jeffrey Lynn Lee

Title Rocket Motor Segmenting

A sub-scale rocket motor segmenting (RMS) capability was developed to support the upcoming demilitarization (demil) requirements for the assets returning from the Warfighter's arsenal and in storage at the various depots. The RMS capability provides the demil community with the option to segment rocket motors into lengths suitable for feedstock to various downstream disposals processes.

The RMS was designed to integrate processes and tooling that are commercially available to eliminate specialization restrictions and a processing time that is surprisingly efficient. The sub-scale development of metal removal processes and the propellant segmenting technique are discussed. Since the RMS provides feedstock, the impact of this technology development has far reaching affects to other demil capabilities. Additionally, missile sustainment requirements benefit equally as this capability provides segments for missile system health diagnostics and analytical data to support stock pile reliability decisions. The production phase of the RMS capability is intended to be depot based and organic workforce user friendly.

Abstract Approval: Committee Chair _____ 2/24/10

Department Chair _____ 3/3/10

Graduate Dean _____ 4/21/10

ACKNOWLEDGMENTS

The completion of my Master's degree would not have reached closure without the support of several individuals. I wish to thank my committee chairman and advisor, Dr. John Gilbert, and my committee members, Dr. Jeffrey L. Evans, and Dr. Ken Zou, for their assistance and guidance throughout this program of study and thesis work. I am grateful for the support of my supervisor, Dr. Robert Little, for providing unrelenting support during my graduate studies and thesis work. Jeffery Wright, a friend for many years and team lead who provided the guidance for this project to come to fruition, to whom I express my deepest appreciation. To the following co-workers for their significant contributions to this effort: John Grisham, Robert Hall, Clint Barnes, Stuart Swint, Josh Hill, and Matt White, to whom I am truly grateful. These individuals shared their time, energy, and expertise to provide valuable assistance in successfully developing a rocket motor segmenting capability from concept to reality. I express appreciation to Mr. Larry Gunter, director of Demil execution, for his patience with the maturation of the rocket motor segmenting technology. Additionally, I am grateful to Chantell Marsh who read the manuscript and offered suggestions to improve the structure and grammatical arrangement of the thesis document.

Above all, I acknowledge un-measurable gratitude for my wife Pam, for 22 years of unconditional love and unwavering support, for believing in my potential and providing unrelenting encouragement throughout the completion of my Master's degree graduate studies.

TABLE OF CONTENTS

Page

LIST OF FIGURES

LIST OF TABLES

Table Page

LIST OF SYMBOLS

D_1	Outer diameter of work-piece
D_2	Outer diameter after metal removal
D	DOC
Ve	Speed in surface feet per minute
N_s	Revolutions per minute
F_r	Feed rate
R	Radius
L_e	Distance of cut
allow	Lead time before and after tool interface w/ material
l_e	Length of the chip
ρ	Density of the steel
SH	Specific heat
V_c	Chip velocity
V_s	Shear velocity
L_c	Chip contact with rake face
W	Width of tooling
W_c	Weight of the chip
w_1	Unformed chip thickness
t_1	Uncut chip thickness = fr
t_2	Cut chip thickness
α	Back rake angle
ϕ	Shear plane angle

ψ	Shear lamella
RF	Resultant force acting on the back of the chip
R'	Resultant force acting on the shear plane
F_{fr}	Friction force
NF	Normal force acting on the tool/chip interface
F_s	Shear force acting on the shear plane
F_n	Normal force acting on the shear plane area
A_s	Shear plane area
F_c	Cutting force
F_t	Tangential (normal force)
β	Friction angle
μ	Friction coefficient on tool/chip interface area
τ	Shear stress
τ_s	Shear stress (flow stress)
E	Efficiency of the machine
CF_s	Correction factor (cutting speed, feed, rake angle
β_1	Boothroyd's exp. curve for proportion of heat conducted back into work-material
a	Width of contact area
b	Length of contact area

Chapter 1

INTRODUCTION

This chapter provides an overview of rocket motor segmenting mission and a brief discussion regarding missile system components. It also presents the fundamental basis for the technology development path, and presents the technologies included in the research work.

1.1 Rocket Motor Segmenting Mission

The Army Product Manager for Demilitarization (PM Demil) has the responsibility for the disposition of all missile systems that have reached the end of their intended service life or have been declared unserviceable. This responsibility drives various technology developments for missile disassembly and disposal. In particular, the Multiple Launch Rocket System (MLRS) demilitarization requirement demands an enormous workload since the Army's inventory is rather large.

There are approximately three hundred and fifty thousand MLRS rounds that will require demil starting in 2012 and will continue for approximately ten to fifteen years thereafter. To support the large MLRS inventory disassembly and disposal requirement, both the commercial industry and the Army organic workforce will provide disposal capabilities (1).

The rocket motor segmenting approach is an Army based technology that will be utilized by the organic workforce to support the MLRS disposal. Additionally, it is anticipated that this technology will be applied to other Army and other service missile (OSM) systems. The primary focus of the rocket motor segmenting (RMS) is to segment

rocket motors into predetermined lengths suitable for specified downstream processing of the metal and propellant components. By reducing a motor into segments, advantages become available for material handling methods, propellant removal processes, as well as providing a means for recycling.

1.2 Fundamental Basis for the RMS Development

The disassembly of the missile system may seem logical in the sense that if the missile can be assembled, then disassembly should be the reverse. Unfortunately, this often elementary synopsis turns out to be a badly miscalculated assumption.

The development of a missile system is often managed independently of other missile systems and from a specific program office within the military services. Therefore, each missile that is designed, fabricated, assembled, tested, and deployed seldom follows an identical developmental path.

1.2.1 Rocket Motor Component and Disassembly Discussion

Granted, every missile has the same basic elemental components regarding their characteristic features: a nozzle, flight motor, payload, and internal intelligence. However, the performance requirements are the primary drivers that determine the final makeup of a missile system. Fortunately, there are only a few assembly methods for joining payloads to flight motors to nozzles.

Typically, the payload and flight motor are joined with fasteners that can be removed with low level mechanical processes and often performed manually. The flight motor nozzles are a different scenario. Depending on the flight motor case manufacture process, the nozzle might be fabricated separately, or as a feature of the casing. In most cases where the nozzle is fabricated independently, the assembly process involves

threading the nozzle into the aft portion of the motor case. However, there are rocket motors that are designed with the nozzle feature fabricated as an elemental component of the flight motor case.

For the purpose of this discussion, consider two missile systems: the Multiple Launch Rocket System (MLRS) and the Tube-launched, Optically tracked, Wire-guided missile (TOW). The nozzle in a TOW missile is threaded into the flight motor. Similarly, the MLRS flight motor also has a threaded nozzle.

The Army has developed a disassembly capability for the TOW missile. Data collected from this disassembly method indicates that 1% of the nozzle threads will seize up during the unthreading process. In this situation, the only recourse is to dispose of the flight motor assembly via open burning which destroys the entire asset and eliminates any opportunity to recover, reuse, or recycle any of the materials and components. The magnitude of this statistic has far reaching implications. There is approximately 5 pounds of propellant in a TOW flight motor while an MLRS flight motor contains approximately 216 pounds of propellant.

When considering the aforementioned inventory in Section 1.1 of the MLRS that will require demilitarization and assuming the 1% failure rate for TOW missile would be consistent for the MLRS, attempting to unthread the MLRS nozzle does not make sense, as this would constitute an enormous work loading of open burning. Given the situation where the nozzle is a fabricated feature of the flight motor casing, careful study of the manufacture method often yields a cut location suitable for gaining access to the rocket motor propellant.

The segmenting process is independent of the unthreading failure issues and provides a safe predictable and repeatable alternative for sectioning the flight motor. The final step to complete the disassembly is to separate the propellant from the motor casing.

There are typically two methods by which propellant is loaded into the motor casing. Depending on performance requirements for the missile system, the propellant can be pre cast and cartridge loaded or the propellant can be mixed, poured into the motor casing and cured to specifications.

The disassembly procedure can be quite simple for cartridge loaded propellant grains. After the motor casing is segmented, the propellant grain is simply mechanically extracted. However, in the case of a case bonded (cast) propellant, the extraction process includes several additional steps to complete the procedure. After the metal segmenting process is completed, the propellant must be segmented as well.

1.2.2 Motor Casings

Each test specimen for the RMS carries unique characteristics that require tailoring of the tool set to accomplish the segmenting process. Presented in this section is a basic discussion about the make-up of each component.

Metal and propellant segmenting are two totally unique processes yet are combined as sequential events on the RMS. This presents challenges regarding thermal response control, chip management, propellant contamination of the metal chips as well as the entire RMS footprint.

Primarily, the focus on metallurgy for the RMS is driven by specimen type. The majority of the work to develop the RMS was focused on the 4130 steel used in the MLRS rocket motor case for two reasons. First, the 4130 steel presents the most difficult

process to overcome due to the manufacture specifications for the motor case. Secondly, the demilitarization work load demand for the three hundred and fifty thousand rounds that will soon reach the end of their service life will mandate that certain capabilities must be in place to meet this requirement. The 4130 steel alloy metallurgical composition is included in Table 1.1.

Table 1.1: Representative Composition of 4130 Steel. (2)

Element	Weight %
C	0.28-0.33
Mn	0.40-0.60
P	0.035
S	0.04
Si	0.15-0.30
Cr	0.80-1.10
Mo	0.15-0.25

Interpreting the call-out for the specifications in the engineering drawings for the motor casing, the American National Standards Institute (ANSI) standard AMS-H-6875 Heat Treating of Steel Raw Materials (3) was the guideline used to develop the structural integrity in the mechanical properties to support the performance parameters of this flight motor. Heat treating 4130 steel can reach Rockwell C (Rc) hardness as high as 42-45.

A hardness test was conducted on a 2” x 1.5” test specimen extracted from an un-fired motor section to validate the specifications in the engineering drawings. The indenter markings were taken on the inner diameter of the case and the results indicated Rc hardness of 42-43 (through hardness). The machinability of the 4130 steel alloy is defined by the level of difficulty regarding the removal of metal related to the amount

energy required or level of shear stress involved (4). The machinability of 4130 steel alloy is typically 70% (5). The 4130 steel alloy test specimens were 0.160” thin walled, cylindrical tubes, 6 feet long, and 8.91” outer diameter.

Chapter 2

LITERATURE REVIEW

This chapter provides an overview of the technology inclusions in the research work. Presented are brief descriptions of industrial usage of each technology, research findings on relevant subject matter, as well as potential applicability to the RMS process.

2.1 Technology Inclusion

Efforts for the RMS capability have focused on the identification, modification (if required), and down selection of a commercially available and suitable technology for safe and efficient processing of rocket motors. Within the technology down selection are lathe type machining, water jet segmenting, laser cutting, and broach/saw cutting. Each of these four metal removal technologies was evaluated in a decision matrix of feasibility, facilitization cost, and efficiency.

The results of the decision matrix eliminated laser and saw/broach cutting due to cost and feasibility, respectively. Currently, the lathe machining and water jet segmenting continue to be the focus of further research.

Several tests and demonstrations with roller wheel and lathe machining have been successfully completed. However; final down selection of the two remaining potential segmenting technologies is pending further research and test results. Predominately, the work and data provided for this thesis is focused on the roller wheel and lathe machining.

2.1.1 Water Jet Segmenting

Recently, water jet segmenting was successfully demonstrated at the Redstone Arsenal (RSA), Huntsville, Alabama, with conclusions compiled in a final technical

report dedicated to that effort (6). The water jet segmenting (WJS) technology uses high pressure, high velocity water and grit to blast away the surface of the part. WJS was included as a potential technology candidate because it has several potential advantages. There are multiple documented projects that outline and discuss successful demonstrations regarding ammunition component demil through the utilization of WJS. The WJS operation can be precisely controlled, provide efficient cutting times, and host the appearance of low facilitization requirements.

Gradient Technologies® was selected to demonstrate the water jet cutting process at RSA on a MLRS rocket motor. The prototype equipment that was demonstrated at the RSA required approximately five hundred internal square feet to function properly. In addition to the internal square feet requirements, the external equipment is mobile for this prototype capability demonstration.

The WJS system that was used by Gradient Technologies is a transportable unit. This system has been successfully demonstrated by Gradient Technologies® for on-site disassembly/disposal of munitions items at several different government sites. While water jet cutting is considered a type of machining process, for clarity and designation, the WJS will be referred to in this document as a separate technology from that of the lathe and roller wheel machining.

2.1.2 Radial Lathe Segmenting

The lathe machining process incorporates a device that is currently being utilized by the petroleum industry for pipe cutting. Pipe cutting technology is well defined by industry, and the radial lathe provides a great deal of flexibility, cost efficiency, and productivity benefits.

Contrary to typical lathe machining, this pipe cutting device rotates the cutting tool while the part remains stationary (radial lathe). This technology is currently being utilized by the Weapons Development and Integration (WDI) directorate on various missile systems for segmenting research that includes ferrous, non-ferrous, and composite case matrixes. The radial lathe segmenting (RLS) approach was included in the technology down selection because the motor case metallurgy, specifically 4130 steel (Rockwell hardness 40-45), lends itself to this type of machining.

Hot tooling creates an unfavorable condition for the RMS. The heat generated in the shear zone must stay with the chip. If the cutting speed is too slow, heat transfer to the tooling is increased based on the dwell time of the chip on the tool. While the dwell time is on the order of milliseconds, there is potential for elevating the temperature of the tool. Proportionally, as the ratio between the depth of cut and chip thickness decreases, the dwell time of the chip on the tool also increases (7).

Decades of theoretical and experimental analysis have been compiled related to orthogonal machining. Chip formation is just one focal point for characterizing the machining process. With the development of micro-imaging, the dynamics of chip formation and tool interface can be understood with much more clarity. Figure 2.1 is a general model of orthogonal machining.

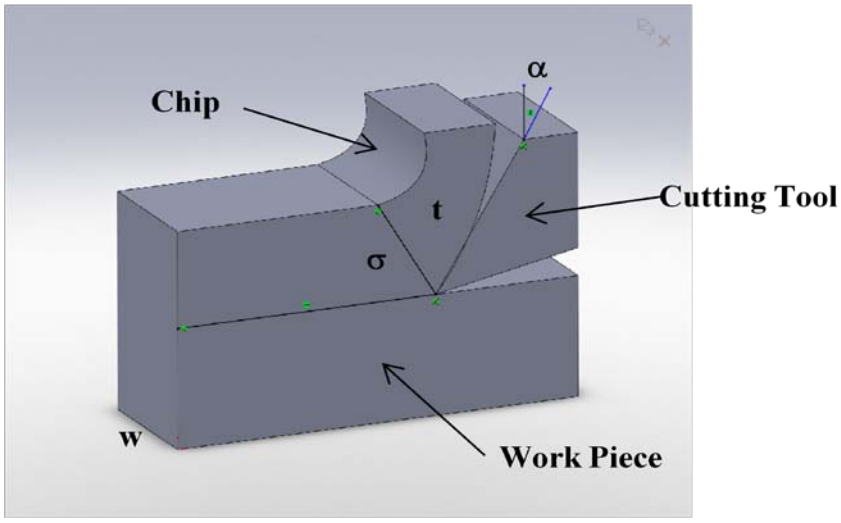

Figure 2.1: Model of Orthogonal Machining

Using this general diagram, evaluation of velocity diagrams (8), finite element simulations of machining (9), stress distribution (10), modeling of cutting forces (11), and temperature prediction (12) have been investigated and provide relevant data for the development of the RMS. Because the RMS involves propellant, temperature profiles for the cutting arrangement are the predominate constraints. With that said, tool, chip, and work piece temperature play a critical role in the segmenting process.

2.1.3 Roller Wheel Segmenting

Roller wheel segmenting (RWS) is a well developed technology that is still being utilized by commercial industry for cutting thin walled cylindrical materials. The idea of segmenting rocket motors without generating hot chips, as with lathe machining and a significant water waste stream as with (WJS), presents an intriguing alternative for the RMS.

Typically, this type of pipe cutting is applied on highly ductile materials where cold forming does not require high force loads. In the case for RMS, there is a large range of

steel and aluminum alloys available among the various rocket motor geometries as well as composites.

Heinrich Hertz introduced the subject of contact mechanics in his paper on the contact of elastic solids in 1881. Hertz restricted his theory to frictionless substrates and perfectly elastic solid material. His theory basically set idol until the beginning of the 20^{th} century after interest was driven by the railway industry (13).

Typically, characteristic assumptions are made in the solutions for calculating the stresses and deformations of blunt edge roller wheel geometry. These assumptions generally include isotropic and fully elastic material, contact areas that are flat and very small, and the two contact bodies that have smooth surfaces (14). Publications on contact mechanics are few and specific topics like roller wheel mechanics are sparsely documented.

2.1.4 Laser Segmenting

Laser machining is a temperature dependant process. Lasers offer a fantastic capability for precision and accuracy for cutting a variety of substrates. Depth of cut can be controlled by manipulating the focus beam and furthermore, intricate profiles are possible using this technology that otherwise, are not possible through conventional technology.

The process for laser cutting includes phase changes in the substrate such as melting, vaporization, and chemical degradation. Using a high energy density focus beam can induce thermal energy into the substrate. As the substrate absorbs the energy, the phase changes are initiated. The molten material is usually removed from the kerf with high pressure gas (15).

Kerf width is a critical element for the propellant segmenting portion of the RMS. Directly related to kerf width is the quality or predictability of laser cutting. The quality of laser cutting is difficult to predict. Contributions from kerf width, surface roughness and the heat affected zone typically characterize the quality of the cut. Rajaram, Sheikh-Ahmad, and Cheraghi (16) suggest that when cutting ferrous alloys in the presence of oxygen gas, oxidation reacts with iron and other alloying elements. This adds another source of heat such that material removal occurs at two moving fronts; the oxidation front and the laser beam front. If optimum cutting speed is maintained, then thermal balance can be established between the two fronts. Otherwise, thermal instabilities rise and the quality of kerf width and surface roughness is reduced (16).

Laser assisted machining is an alternative for extending tool life. In this arrangement, the laser beam is focused and guided along the cut line and ahead of conventional tooling. The purpose of laser assisted machining is to preheat the kerf and soften the substrate to create a ductile material removal process that reduces the stresses on the conventional tooling (17). Using laser assisted machining, Ding and Shin (17) successfully demonstrated the absorptivity of AISI 4130 to be approximately 0.43. The heat absorption created a cutting environment with temperatures up to 572^{o}F and a 20% reduction in specific cutting energy.

The literature review revealed that laser cutting is an applicable technology for the metal removal portion of the RMS. However, the high end temperatures complicate the process in the environment of propellant. Laser segmenting was eliminated in the down selection process due to the anticipated capital cost and the potential high maintenance risk associated with the production environment where the RMS must function.

2.1.5 Broach/Saw Segmenting

Broaching and sawing were categorized together due to their functional similarity. These technologies are fairly low maintenance and, typically, cost effective. During the concept evaluation of the segmenting process using these technologies, the realization that the curl of the teeth often returns through the medium with chips embedded raised safety concerns.

In the metal removal process of thin walled tubes, the amount of material remaining in the bottom of the kerf tends to be 0.004” to 0.05” depending on the feed rate of the tooling. This thin strip of metal has been termed the wedding band.

At the interface between the wedding band and the propellant to the teeth on the broach/saw there are concerns for pinch points. Therefore, concerns for feasibility of establishing a safe and repeatable capability eliminated these technologies from the final down selection.

2.2 Propellant Segmenting

Due to the confidentiality of some propellants, their chemical make-up will not be included in this paper. Although each has a unique make up, the density of solid propellants tends to vary marginally and works advantageously for the RMS process. The texture of the propellant is critical to proper cutting technique.

There are inheritable issues associated with cutting propellant. The potential for electrostatic build-up and discharge (18), high pressure pinch points, heat generation, and mutilated surface of the propellant (19) are among the most critical.

The mechanics of cutting pure propellant are very basic. Guillotines, band saws, mills, and piano wire are very common devices and all require the propellant to be

exposed. Piano wire is a common tool for segmenting propellant, and wire diameter may vary depending on the density and physical characteristics of the medium. An automated mechanism exists for forcing the wire through the medium, but the process can be successful using a manual set up.

The RMS process utilizes the wire process to segment the propellant after the metal is removed. The missile systems under consideration for RMS are obviously solid propellant. Solid propellants have nearly the same physical characteristics and often have similar appearances. Their consistency is similar to that of a pencil eraser.

2.3 Thermal Imaging

There are many techniques that attempt to measure the temperature in the cutting zone. Thermocouples, sensors, thermo-vision or inferred cameras and metallographic techniques are just a few of the methods or devices that have been integrated into the cutting environment to capture and develop chip-tool thermal profiles. Research conducted by Kwon, Schiemann, and Koutanya (20) revealed that when using infrared cameras with TiN coated inserts, emissivity is greatly affected by the coatings.

Favorable to the RMS metal removal process, the TiAlN inserts characteristically have low heat conductivity and force the heat energy into the chip. Although the low emissivity of the insert degrades the thermal profile of the insert, the choice to use an infrared camera for the RMS temperature profile development was primarily to focus on the temperature of the kerf.

Another method for observing temperature is the coloration of the chips. As the chips leave the tool rake face at the temperature range as previously mentioned, their coloration changes to blue or brown. This is typical when machining without coolant.

Chapter 3

EXPERIMENTAL METHODS

3.1 Objectives and Scope

The research objective of this thesis is to determine a suitable technology to modify and adapt into a process for segmenting rocket motors. This chapter presents an overview of the scope of experimental methodologies for developing the RMS capability through the technology inclusions as stated in Section 1.3.

3.2 RMS Overview

The requirement for the RMS is to create a circumferential opening (kerf) in the motor case at a desired location that is geometrically suitable to allow for follow-on segmenting of the propellant. Due to the potential for igniting the propellant, temperature is a major performance parameter for the RMS.

The experimental methods are characterized as non chip forming and chip forming machining processes. There are two devices that form the foundation for the experimentation. A horizontal lathe was used for the lab-scale RWS effort and post lab-scale, the radial lathe equipment was the base unit for both the non chip forming and the chip forming machining processes.

3.3 Non Chip Forming Machining Test Set-up

The purpose of the RWS tests was to evaluate and determine the applicability of the roller wheel cutting as a means to develop tooling and a process to facilitate the RMS. Ideally, the preferred technique would eliminate chips from the metal cutting operation and have a minimum thermal gradient.

With the RWS, the tool speed and feed are similar to lathe cutting, so the operational parameters are somewhat consistent with lathe machining. There were two separate test configurations conducted with the RWS concept. The first series of tests was conducted as a proof of concept in a lab scale environment and was demonstrated on a rather large horizontal lathe. The second series of test was conducted using the radial lathe.

Both lathes were selected because of their mechanical rotation capability. To form a basis of expectations regarding the performance of the roller wheels, the following general mathematical models by Ugural and Fenster (14) were used. Figures 3.1 and 3.2 illustrate the loaded configuration of the wheel.

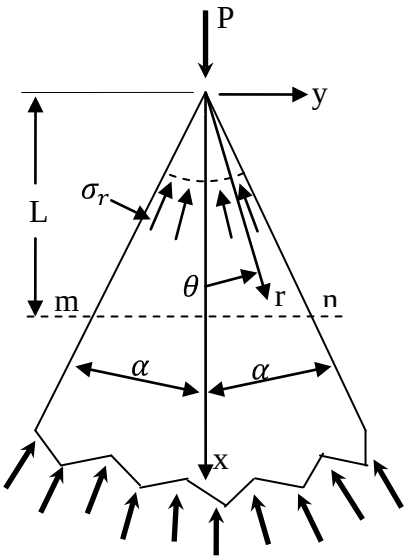

Figure 3.1: Point Load on a Wedge.

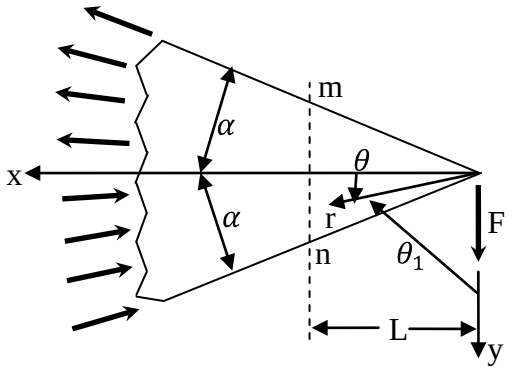

Figure 3.2: Cantilever Load on a Wedge.

The point load at *P* puts the wheel in a state of compression. The stress vector, σ represents the stress distribution in the web of the blade at a distance from the point. The angles of the stress concentration from the center of the blade to the outer edge are represented by θ and length, *r*. The thickness of the blade is represented by the half angle, α.

A quick study of Figure 3.1 indicates that the normal stress maximizes as θ approaches 0 and *r* decreases and minimizes at $\theta=\alpha$. These particular stress concentration points are critical to the RWS.

Equation 3.1 satisfies the stress distribution resulting from the point load on the wheel. The maximum contact pressure is represented by Equation 3.2 where *b* (Equation 3.3) is width and *a* (Equation 3.4) is the length of the contact between the two surfaces. The radii of the two surfaces are represented by r_1 and r_2.

$$\sigma_r := \frac{-P\cdot\cos(\theta)}{r_w\cdot\left[\alpha + (.5\cdot\sin(2\cdot\alpha))\right]} \tag{3.1}$$

$$\sigma_{max} := \frac{2\cdot P}{\pi\cdot b\cdot a} \tag{3.2}$$

$$b := \left[\frac{4\cdot P\cdot r_1\cdot r_2}{\pi\cdot L_c\cdot(r_1 + r_2)}\cdot\left(\frac{1-\nu_1^{\,2}}{E_1} + \frac{1-\nu_2^{\,2}}{E_2}\right)\right]^{\frac{1}{2}} \tag{3.3}$$

$$a := Ka \cdot P^{\frac{1}{3}} \tag{3.4}$$

Additionally, if the point load is applied at 90^o from the point, the wheel will be cantilevered. In this case, tension and compression are present in either the x or y direction depending on the location of the *Lc* along *x*. At 45^o, τ_{xy} is a maximum. The following equations satisfy the stress distribution in the cantilevered condition.

$$\sigma_x := \sigma_r \cdot \cos(\theta)^2 \tag{3.5}$$

$$\sigma_y := \sigma_r \cdot \sin(\theta)^2 \tag{3.6}$$

$$\tau := \sigma_r \cdot \sin(\theta) \cdot \cos(\theta) \tag{3.7}$$

3.3.1 Lab Scale Test and Set Up on the Horizontal Lathe

The set-up included a 192" Alexon lathe, a modified tail stock, and specifically designed tool holders. The extended length chuck jaws on the lathe were manufactured uniquely for flight motor test and operations. The tail stock formed the structural basis to mount a 3-jaw, self-centering chuck. Mounted onto the 3 jaws of the tail stock chuck were tool holder devices specifically designed for disk-type, pipe-cutter wheels.

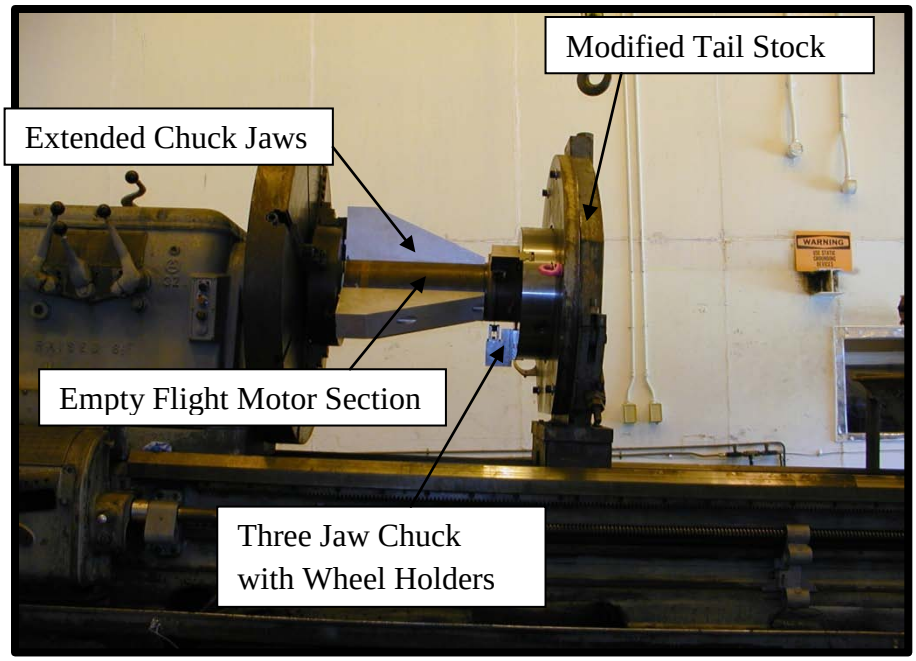

Figure 3.3: Lab Scale Set Up for the RWS.

In the test arrangement, the motor case was held in position by the lathe chuck and rotated very slowly. The roller wheels were indexed into the rotating motor case manually according to the test plan. Figures 3.3 – 3.7 illustrate the interface between the roller wheels and the empty flight motor casing. Figure 3.8 illustrates the tooling array used in the horizontal lab scale tests.

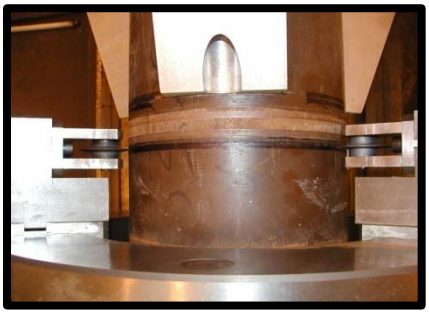

Figure 3.4: Top View of RWS Test Set Up.

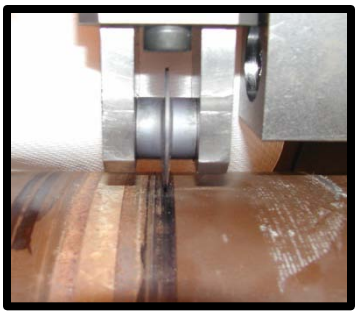

Figure 3.5: Front View of RWS Set Up.

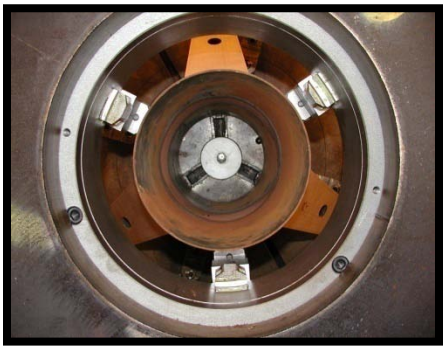

Figure 3.6: End View of RWS Set Up.

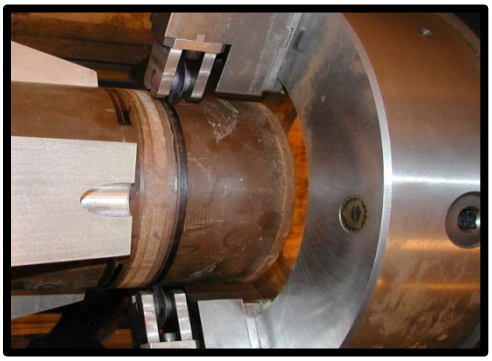

Figure 3.7: Isometric View of RWS Test Set Up.

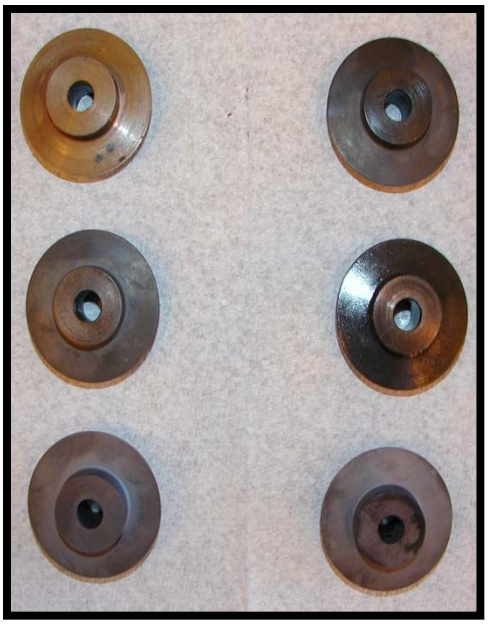

Figure 3.8: Tooling Array for Lab Scale Tests.

3.3.2 Lab Scale Test and Set Up on the Radial Lathe

The second series of test was conducted with the radial lathe. This particular lathe is used in the commercial pipe cutting industry for both roller wheel cutting and lathe tool cutting. Tool holding fixtures are readily available from commercial off the shelf (COTS) suppliers.

The radial lathe is unique in application because it clamps onto the specimen and thus reduces the requirement for elaborate support fixtures and hardware. Figures 3.9 and 3.10 illustrate the test set-up.

The procedure for setting up this RWS arrangement includes a test specimen loaded and clamped into an I-beam support structure and the installation of the radial lathe onto the specimen. This step aligns the RWS with specimen and perpendicularly to the intended cut line. With the lathe in place, the tool slide (tool holding fixture) is installed on the lathe and finally, the roller wheel is bolted onto the tool slide.

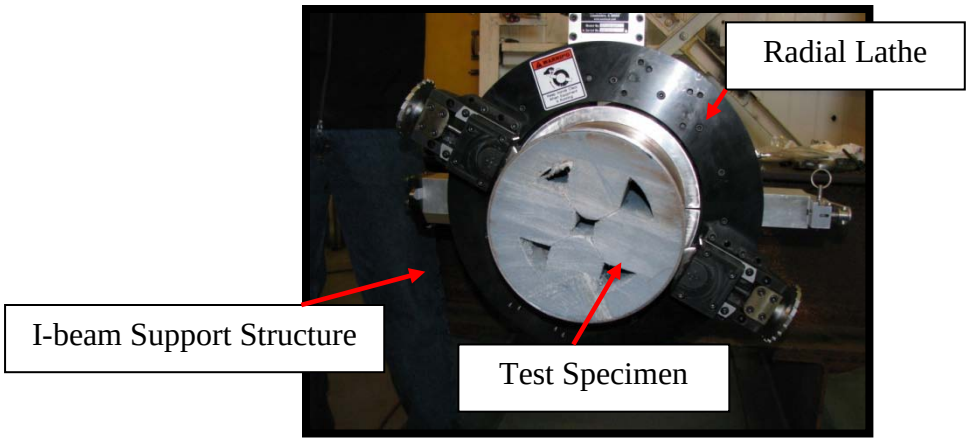

Figure 3.9: RWS on Radial Lathe.

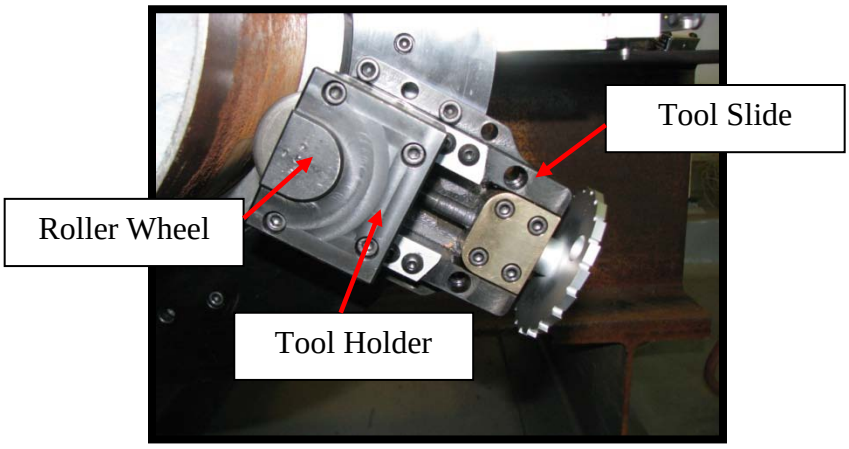

Figure 3.10: Tool Slide and Roller Wheel Holder.

The lathe can be operated pneumatically or hydraulically. Hydraulic drives are preferred and tend to provide smooth, uninterrupted power. As power is supplied to the drive motor on the radial lathe, the tooling is rotated about the circumference of the motor casing. With each rotation, the tooling is indexed into the motor case. The feed rate of the tool depends on the threads per inch of the tool slide drive screw. To manipulate the radial lathe's basic operational parameters, the drive motor speed and the feed screw must be altered. Figure 3.11 is a model of the tooling profile selected for the RWS testing and are characterized as the typical full angle roller wheel used by industry every day for parting ductile tubing. This model is 2.5" in diameter and has a 45^{o} attack angle.

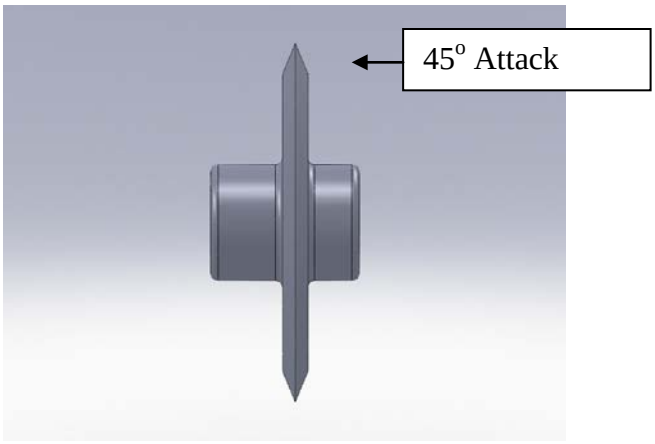

Figure 3.11: Roller Wheel Model

3.4 Chip Forming Machining Process and Set-up

In chip formation, the intensity and amount of heat is proportional to the operational parameters of the machining process (tooling, speed, and feed rate) and specific to specimen metallurgy. Heat is induced from the energy required to force the tooling into the metallurgic grain structure of the specimen. As a thin layer of metal is removed (chip formation) between the tooling and the specimen, the heat is dissipated from shear plane and into the chips.

Formation and condition of the chips is driven primarily by tool geometry, the speed of the cutting motion, the feed rate that the tooling engages the specimen, and the amount and type coolant or lubricant used. There are two methods for chip forming included in the development of the RMS and they are the WJS (considered a chip forming process) and the lathe machining. The challenge with this methodology is finding a set of parameters that fits the requirement to machine away the metal and not excite the propellant.

3.4.1 Lathe Machining Test and Set-up

The mechanical structure and method of operation of the pipe cutter provides the flexibility for demonstrating chip and non chip forming cutting operations. Subscale operations, utilizing existing hardware at RSA, consist of a test fixture to hold the rocket motor, a radial lathe (pipe cutter), and power supply.

The test fixture is configured in such a way that it will support the specimen during segmenting operations. An advantage of the pipe cutter is that it mounts onto the specimen. Therefore, no additional fixtures are required for this scale of work.

As power is supplied to the drive motor on the radial lathe, the tooling is rotated about the circumference of the motor casing. Figure 3.12 illustrates the subscale test arrangement. With each rotation, the tooling is indexed into the motor case. The feed rate of the tool depends on the feed screw threads per inch. To manipulate the radial lathe's basic operational parameters, the drive motor and feed screw must be altered.

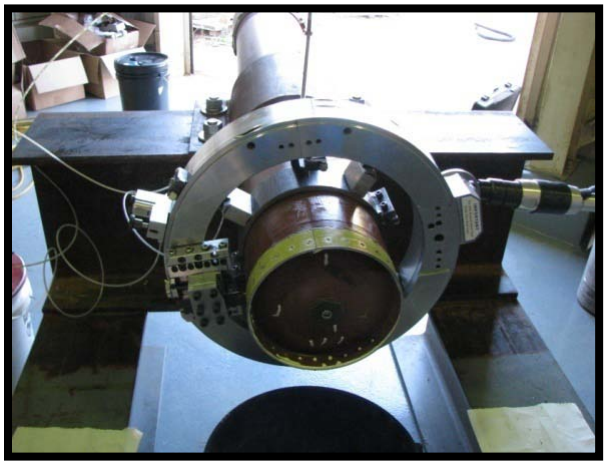

Figure 3.12: Radial Lathe Test Set Up.

3.4.2 Temperature Profile Development

Due to the sensitivity of the RMS, it is imperative that good thermal data is collected to verify the real time status of the thermal relationship between the machining operation and the propellant. The challenge with this set-up is the final interface of the tooling with the propellant.

As the tool finally removes the wedding band, the temperature of the tooling becomes paramount since the propellant is exposed.

A tremendous effort was expended in developing a thermal profile through the tool selection and operational parameters variables. Equation 3.8 provides an iterative approximation for a range of temperatures expected based on operational parameters.

$$\Delta T := \left[\frac{\left(F_c \cdot \cos(\phi) - F_{fr} \cdot \sin(\phi)\right) \cdot \cos(\alpha)}{\rho \cdot sh \cdot w1 \cdot t_1 \cdot \cos(\phi - \alpha)} \right] \cdot (1 - \beta 1)\,(21). \tag{3.8}$$

The iterative values of cutting force, F_c is given a range based on tool selection and parameters. The variables, $\Phi, \alpha, \rho, SH, w_1, t_1$, and β_1 are constants and F_{fr} is a dependant variable on F_c.

Equation 3.8 characterizes the heat in the primary shear zone between the chip and rake face of the tooling. Generally, the chips reach a temperature range of 390^{o}F to 660^{o}F in steel machining operations. This temperature range becomes critically important when compared to the auto-ignition temperature of the propellant.

The thermal imaging equipment used to monitor the machining operations was a VarioCam® Inferred (IR) digital camera. Data collected with the IR camera was used to input data for Equation 3.8 to generate a theoretical range of force data. Additionally, the force data was input data for the calculation of the theoretical point loads on the wedge (roller wheels) and also the cantilever loads in the roller wheels.

3.5 Tool Selection

Tool selection for the subscale testing of the non chip forming and chip forming segmenting processes included the investigation of various kerf widths, tool insert geometry, coolant types, cutting speeds, feed rates, and temperature data for the metal removal processes. The kerf (cut width) is critical, since this cut through the metal casing makes room for the follow-on propellant segmenting process.

Tooling for the RWS included an array of various wheel diameters, web thickness, and point radii. Tooling for the RLS included four different geometries of tool inserts. Selections were chosen based on in-house knowledge, industry consultation, and segmenting requirements. The inserts are a titanium aluminum nitride alloy (TiAlN). Table 3.1 contains the four inserts and their kerf widths for the initial test plan for kerf formation.

Table 3.1: Tooling Insert Kerf Widths.

Designation	Material	Kerf (in)	Chip Breaker
J02	KU25T	.087	Medium
J03	KC5025	.118	Medium
J05	KC5025	.197	Medium
J06	KC5025	.236	Medium

Obviously, temperature data is critical considering the nature of this process. Along with operational parameters and specimen metallurgy, tooling coolant is vital to the

service life of the equipment and also assists in controlling the temperature gradient from the tooling to the specimen. Several coolant types have been investigated and include water based mixes, liquid nitrogen, nitrogen gas, and compressed air.

Additionally, RLS tests were performed with no coolant. This is an important concept since the downstream processing of the propellant could possibly prohibit the introduction of contaminants. Some propellant will absorb moisture and other compounds when exposed. Therefore the RMS must meet the requirements for propellant integrity.

The thermal imaging camera was utilized for remote, real-time collection of temperature data during the segmenting processes. Initially, an inert MLRS section was used to demonstrate cutting performance on kerf geometry related to the various chip forming tooling inserts.

3.6 Propellant Segmenting

This section presents a discussion on the methodology for segmenting propellant after the kerf is formed. Wire cutting propellant is a fairly mature process.

Typically, the wire is looped over the motor and into the kerf and finally, terminating into a flat plate below the motor. The plate is then loaded with weights. As the mass increases on the plate, force is transferred through the wire and forces it through the propellant.

This system is effective; however, it is somewhat cumbersome and slow. The RWS and RLS tooling for cutting propellant provide automation for the wire cutting process.

Two wires are looped into the kerf: one on the top side of the motor and the other on the bottom side. The wires have formed ends using cable thimbles. The thimbles are

attached to compression springs that have hooks at the ends. The springs are mounted on the rotation face plate of the radial lathe. Figure 3.13 illustrates the inert propellant segmenting apparatus and IR camera.

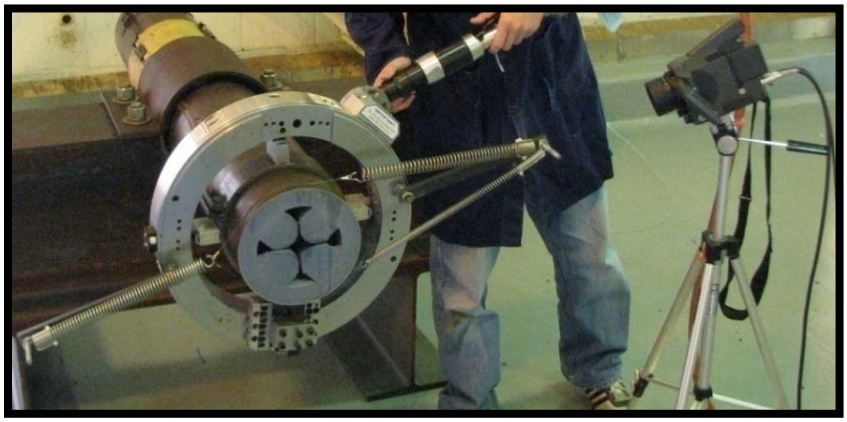

Figure 3.13: Propellant Segmenting Set Up.

The radial lathe is actuated and while rotating, the wires cut through the propellant. The wire is a patented, omni-directional saw. Two sizes of wire diameter were used in the subscale effort. Their specifications are listed in Table 3.2.

Table 3.2: Wire Saw Specifications

Specification	Saw #1	Saw #2
Diameter	0.0276”	0.039”
Length	12”	12”
Pull Test Max	140 lb	358 lb

Chapter 4

RESULTS AND DISCUSSION

4.1 Executive Summary

This chapter presents and discusses the experimental results related to non chip forming, chip forming and propellant segmenting. The work focuses on conventional technology for pipe cutting and wire sawing with adaptation to machining carbon steel rocket motor cases, and the cutting of rocket motor solid propellants.

The migration from lab-scale concepts to prototype-scale datum are developed in this chapter. The motivation for the experimental effort was driven by the thrust of the quickly approaching MLRS demil workload and provides the basis for the primary RMS focus on the 4130 steel alloy motor case.

4.2 Non Chip Forming

Idealistically speaking, accessing the solid propellant inside the motor case without creating metal chips offers advantages regarding propellant contamination. Usually, this type of metal cutting has a low temperature profile compared to the lathe machining. Furthermore, eliminating the operational housekeeping associated with chip forming methods creates a favorable scenario for non chip forming techniques.

4.2.1 Horizontal Lathe Roller Wheel

The initial research and development effort put forth regarding a RWS capability was conducted on the horizontal Alexon lathe. Results from this inert testing were unfavorable.

While roller wheel cutting is a well develop technology, the effort expended in this project yielded marginal results. A motor case was not successfully segmented during any of the tests.

The first series of tests involved only one roller wheel as this was the anticipated approach for the RMS. The engagement between the roller wheel and the motor case was introduced manually through the 3-jaw chuck. Because the motor case was empty, deflection was immediately initiated due to the side loading from the roller wheel. Not only was deflection an issue, but the motor case tended to walk out of the lathe chuck jaws. This condition presented alignment issues with the roller wheel to the cut line on the motor case. A new score line would form with each rotation of the motor case, basically, threading the outer surface.

In the second series of tests, off-set rollers were added to the tailstock chuck to oppose the side loading of the roller wheel. This aided in the on-set of segmenting, however, still present was the condition where the motor tended to walk out of the lathe chuck. In this condition, transverse loading (cantilever loading) in the roller wheel increased rapidly causing catastrophic failure to the roller wheel edge.

For the third series of tests, three roller wheels were installed into the tailstock chuck. The idea here was to introduce three-point loading thus keeping the motor case on axial center with the lathe chuck and prevent the problem with the motor case walking out the chuck and also to equally distribute the load to the three roller wheels.

The tailstock chuck provided the alignment for the three roller wheels in order for each wheel to engage in the same kerf. Two of the roller wheel holders were shimmed normal to the kerf to create a continuous cutting action for all three wheels.

Initially, this test arrangement yielded improvements for controlling the alignment; however, the deflection issues continued to prevent segmentation. A kerf was formed but the roller wheels would fail catastrophically prior to completing the cut. The failure modes of the roller wheels are illustrated in the Figures 4.1- 4.3. These types of failures were consistent through-out all the tool geometry illustrated in Figure 3.8.

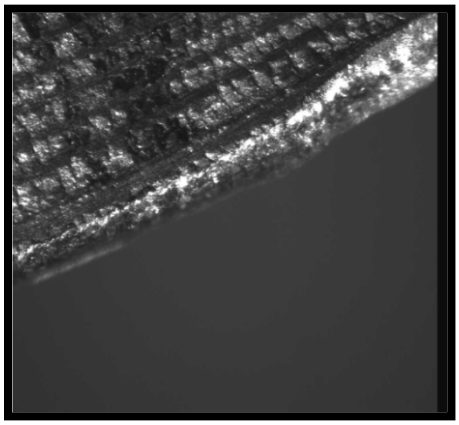

Figure 4.1: Cold Rolling of Roller Wheel Edge.

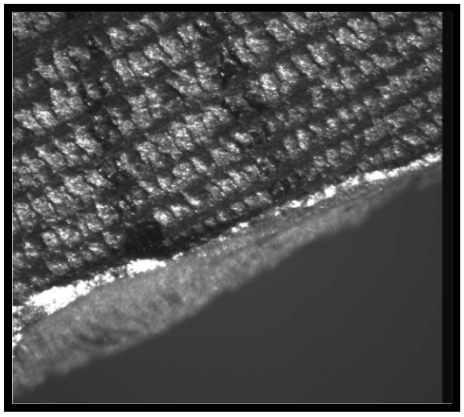

Figure 4.2: Edge Shear of Roller Wheel.

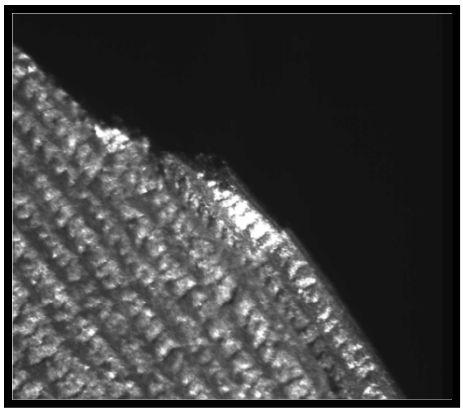

Figure 4.3: Fracture of Roller Wheel Edge.

Failure criteria were attributed to the test apparatus anomalies. The defection in the motor case could not be overcome in the test arrangement.

As a result of the magnitude of the three-point loads, the tailstock assembly moved out of position, further exacerbating alignment issues. The alignment issues eliminated any possibility of repeatability in the test data. After repeated attempts, the approach was abandoned.

4.2.2 Radial Lathe Roller Wheel

After the RWS tests were completed on the horizontal lathe, a more suitable test arrangement was developed to continue the non chip forming segmenting effort. Because of its unique design, the radial lathe offers the ability to manipulate performance variables related to speed, feed rate, and the alignment issues experienced earlier with the horizontal lathe tests.

The speed of the radial lathe is controlled at the drive motor with a flow control valve. The feed rate involved changing the thread pitch on the tool slide drive screw.

Tool geometry was modified to a more robust design. These roller wheels had a larger diameter and an increased web thickness. The attack angles ranged from 22.5^{o} to

45^{o}. The test specimens for this series of test were MLRS rocket motors with inert filler. The inert filler approximates the density of the actual propellant but was non energetic.

The first series of test yielded similar results as with the horizontal lathe tests. The alignment issues were reduced with the radial lathe; however, deflection in the motor case continued as before. The deflection was so great that the entire motor case appeared to be in cyclic torsion (morphing) during segmenting operations.

As the roller wheel rotated about the circumference of the motor case, a reactive deflection translated the entire length of the motor case. The radial lathe behaved similarly with the tendency to walk along the longitudinal span of the motor case. Favorably, the roller wheel did eventually form a shallow kerf.

Because of the longitudinal movement in the radial lathe, the roller wheels once again reached catastrophic failure. In addition to failure at the roller wheel edge, a major shear action occurred near the mid section of the roller wheel web. The edge tip fracture was attributed to excessive forces applied to the hardness of the motor case (Rc 42-44) while the web shear was attributed to the movement in the radial lathe.

The set-up for the second series of tests included an apparatus for loading the test specimen in compression and tension as can be seen is Figures 4.4 and 4.5. A threaded rod was positioned through the bore of the motor case and external plates attached. The plates were tightened against the ends of the motor case to various torque loads. Additionally, loading the motor case in tension was achieved using the same type of apparatus but in the opposite fashion.

Clamps were placed around the motor case and treaded rods attached. As opposing force was applied to the clamps, the motor case was placed in tension. The ideology of

this arrangement was to restrict the morphing of the motor case and make the work surface rigid.

Four tests were conducted and the results are illustrated in Table 4.1. The compression test at 50 ft-lb was a successful segmentation. However, the elasticity in the motor case inert filler caused the kerf to close up after the roller wheel was removed. The catastrophic tool failures in Tests 2-4 are illustrated in Figures 4.6 and 4.7.

Figure 4.4: Compression Test Apparatus.

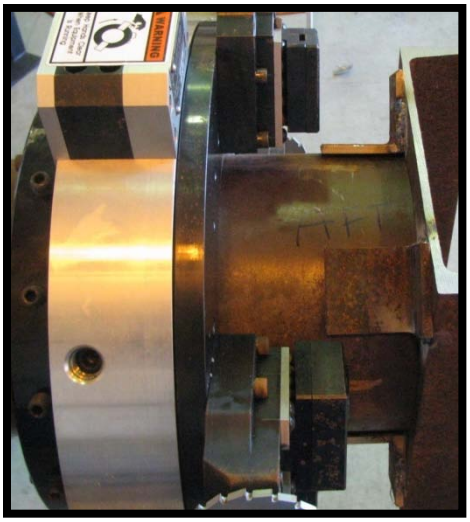

Figure 4.5: Side View of Compression Test Apparatus.

Table 4.1: Compression and Tension Test Data.

Test #	Type	Torque	Result
1	Compression	50 ft-lb	Successful segmentation
2	Compression	75 ft-lb	Catastrophic tool failure
3	Compression	150 ft-lb	Catastrophic tool failure
4	Tension	250 ft-lb	Catastrophic tool failure

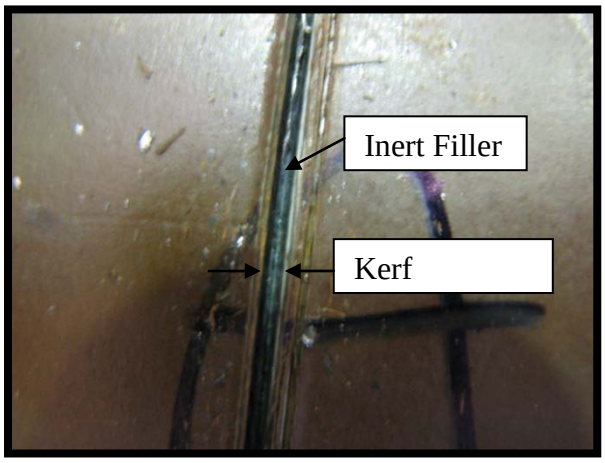

Figure 4.6: Kerf Closure After Segmenting.

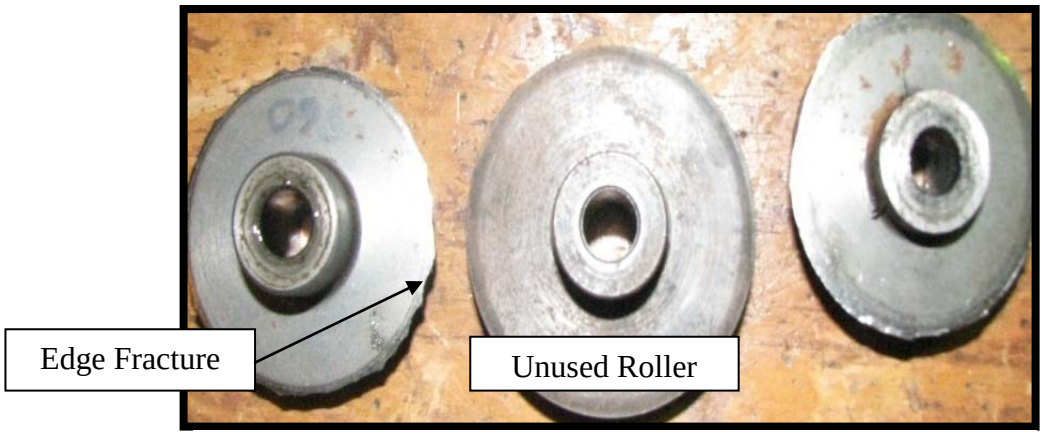

Figure 4.7: Edge Fracture and Unused Wheel.

To overcome the deflection, the third series of tests included a 2 piece clam-shell ring called a rounding shoe. The rounding shoe was specifically designed and fabricated to fit the diameter of the MLRS rocket motor's outer diameter. The purpose of the rounding shoe (as its name indicates) was to force the motor case to become round, rigid,

and reduce the deflection issues during the segmenting process. The rounding shoe is illustrated in Figure 4.8.

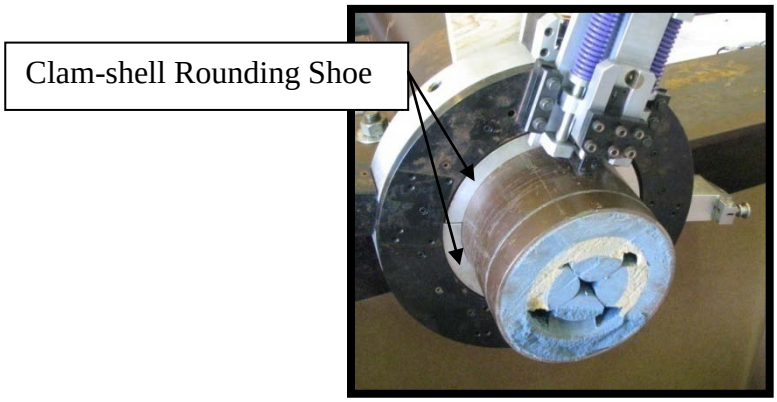

Figure 4.8: Rounding Shoe.

With the rounding shoes attached to the motor case, the radial lathe was installed on the outer surface of the rounding shoe. Several tests were conducted with this testing arrangement and yielded marginal results.

The deflection issues were not eliminated but minimized. However, the roller wheel continued to attempt to thread the outer surface of the motor case but eventually formed a shallow kerf. The kerf depth would vary from one test to the next. Once again, the roller wheels ultimately reached catastrophic failure by fracturing in the mid section of the web prior to completing the segmentation process.

It was determined that even with the rounding shoe, there was still longitudinal movement of the radial lathe occurring during segmentation. A second ring was fabricated for purpose of mitigating the longitudinal movement of the radial lathe.

This lathe stabilizing ring (LSR) was larger than the diameter of the motor case and has threaded holes, equally spaced about the outer circumference. The LSR was positioned tightly against the back face of the radial lathe and held in place with bolts that pass through the treaded holes and apply force on the motor case.

With the addition of the LSR, the fourth test series was consistent with the previous tests with no improvement in the longitudinal movement. The roller wheels continued to shear in the web section.

Since the longitudinal movement of the radial lathe during the test series was predictable and repeatable, the final step to mitigate the movement in the radial lathe was to work around it. An adjustment was made to the tooling profile. The external face of the roller wheel hub was machined to remove enough material to create an open space between the hub and the tool holder. This provided stress relief for the roller wheel during the movement of the redial lathe.

Finally, this arrangement yielded favorable results in Test Series 5. The longitudinal movement was overcome, the shear stress in the roller wheel was reduced and kerf formation for segmentation achieved.

The results from this test series brought to light that the roller wheel was enduring enormous forces in order to compete with the movement in the radial lathe. During the final parting of the metal in the kerf, an auditable, rapid fracture would occur to complete the segmentation process.

The rapid fracture resulted from the compression forces applied to the kerf from the forces on the roller wheel and the countering compression forces applied from the elasticity in the inert filler. Visibility, the kerf would open just ahead of the roller wheel rotation and then close up shortly after the roller wheel pasted through. The inert filler was cast and bonded to the inner diameter of the motor case therefore the surface area is rather large as well as its elasticity and memory. This condition raised serious concerns regarding pinch points in the kerf region. Although RWS had reached a pivot point in

segmenting the 4130 steel alloy, the realization of and concern for the pinch points halted further developmental testing.

4.3 Chip Forming

The purpose of the RMS chip forming effort was to determine if machining the metal and exposing the propellant was even possible. Knowledge and experience needed to be gained at the sub-scale level in order to justify continuance and pursuit of a prototype RLS effort.

Developmental work and testing for RLS was conducted parallel with the RWS tests, since the same radial lathe was used as the drive mechanism for both approaches. During the analysis, design, and fabrication for one effort, the other would be conducting tests.

For the RLS, multiple series of tests were conducted to analyze and determine tool and chip formation, temperature profiles, coolant application, kerf development, and optimization of the speed and feed rate. Thermal imaging was present for collecting the temperature responses and developing a thermal profile between the tooling and the motor case.

The thermal imaging data carried a two-fold criticality. First, this data provided the temperature profile to establish a range for operations and secondly, the temperature range was used to calculate the amount of force loads in the system.

4.3.1 Lathe Machining Segmenting

The first series of tests was designed to determine tool selection. Initially, titanium-aluminum nitride (TiAlN) inserts and T-15 tool steel were the two types of tools selected.

Since kerf width was a critical parameter, the selection included a variety of tool geometry.

Table 4.1 includes representative kerf widths for the initial testing with tooling inserts. The intent of the tests was not to determine the failure modes; however, chipping, breaking, and tool wear were considered important information. After ten repeated cuts of each tool insert, microscopic inspection indicated that the KC5025 had less wear and was most likely the better candidate for higher service life. The smaller kerfs yielded favorable temperature data and cutter performance. Figure 4.9 is a graphic profile of the temperature and kerf relationship. All other variables were constant during insert thermal characterization tests.

Figure 4.9 Insert Temperature Profile

During insert testing, issues associated with the kerf widths and the wedding band were investigated. As previously stated, the wedding band references the thin band of metal that remains at the interface between the propellant and the inner case wall inside the kerf. Near the end of the cutting operation, this band becomes very thin. As the cutting tool rotates around the specimen, the metal band tends to flex under the pressure of the cutting tool, such that the cutting tool slides across as opposed to actually cutting it.

The predictability of removing the wedding band depends on the kerf width. With the smaller kerf widths, cutting continued through the entire removal process with no indication of a wedding band being created. However, with the larger kerf widths, a wedding band was formed.

To remove the band, the cutting tool would continue past the inner diameter of the metal casing until the wedding band deflected enough to form a wrinkle just ahead of the cutting tool. Eventually, the wrinkle became large enough that the cutter engaged and peeled the band out. Figures 4.10 - 4.12 illustrate the wedding band as removed from the motor case.

Figure 4.10: Representative of Wedding Band Removal (0.087").

Figure 4.11: Representative of Wedding Band Removal (0.197").

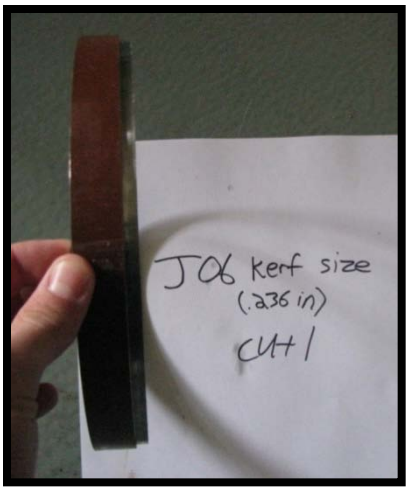

Figure 4.12: Representative of Wedding Band Removal (0.236").

This creates a safety concern with bonded propellant on the inner diameter of the motor case. If the cutting tool is required to continue into the inner diameter, the cutter has to contact propellant as well as metal at the same time. Furthermore, the number of revolutions the tool must make to finally remove the wedding band becomes counter-productive.

In Figure 4.12, the wedding band remains attached to the segmented section of the motor case. In this situation, the tooling continued until the wedding band cold-worked itself to the point of fracture at the right side of the kerf.

During all tests, the rotational speed of the cutting insert and the tooling feed rate were held at a constant rate of 14 revolutions per minute (RPM) and 0.0044” per revolution, respectively. Depending on the initial set point for the tooling, a complete cut on an M26 motor case took approximately 6 minutes. Table 4.2 summarizes a portion of the data collected from the subscale testing. This type of data was collected on each cut and was used for selecting the optimum tooling and speed/feed rate.

The tooling geometry must maintain a significantly lower temperature profile with respect to the auto-ignition of the rocket motor propellant. In the case of MLRS rocket motors, the propellant has an auto-ignition above 450^{o} F.

Figure 4.13 is an image taken of an inert motor case section with the various kerfs created during insert testing. As illustrated in Table 4.2, the temperature profiles generated in the subscale tests were higher than desired but well below this temperature.

These tests were conducted without coolant specifically to establish a true datum for the temperature response of each insert. Although the 0.197" insert creates a thermal profile near the high end of the set, it was chosen for follow-on testing due to applicability to the propellant segmenting process where kerf width is critical. Appendix A contains several graphs illustrating the coolant based tests that were conducted to develop a thermal profile for the RLS.

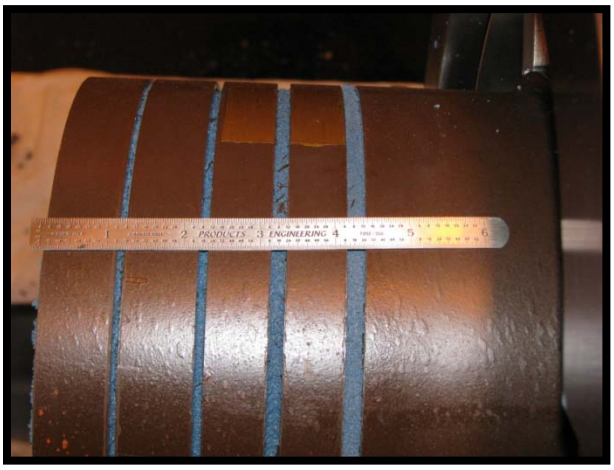

Figure 4.13: Representative Kerfs.

Table 4.2: Representative Data for Insert Tests

Test	Vendor Designation	Kerfs	Chip Breaker	Material	# of Cuts	Maximum Temp. °F
1	J02	.087 in	medium	KU25T	3	242.9
2	J03	.118 in	medium	KC5025	3	279.9
3	J05	.197 in	medium	KC5025	3	299.3

4	J06	.236 in	medium	KC5025	3	358.2
5	J02	.087 in	fine	KU25T	3	221.1
6	J02	.087 in	medium	KU25T	3	242.9
7	J02	.087 in	course	KC5025	3	220.4
8	J02	.087 in	medium	KU25T	10 (7)	289.7
9	J03	.118 in	medium	KC5025	10 (7)	323.1
10	J02	.087 in	medium	KU25T	1	236.9
11	J03	.118 in	medium	KC5025	1	311.1
12	J05	.197 in	medium	KC5025	1	299.8
13	J06	.236 in	medium	KC5025	1	328.5

Oil based coolant was eliminated early on due to the complications of maintenance in the production environment. Cryogenic coolant has been determined to extend tool life, improve surface roughness, reduce friction and cutting forces (22). A device was fabricated to provide liquid nitrogen (illustrated in Figure 4.14) as a coolant but was eventually rejected due to feasibility and cost.

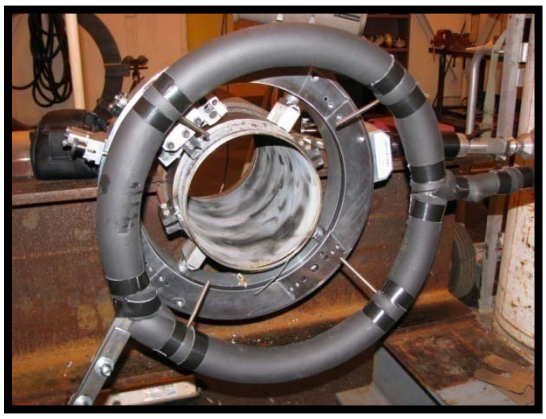

Figure 4.14: Nitrogen Coolant Apparatus.

Although a variety of coolants were tested, a continuous water-based lubricant was selected and used predominately throughout the RMS development. Data specific to the coolant analysis are graphically illustrated in Appendix B.

Several segmenting tests were successfully completed using the RLS with the 0.097" insert. The performance of the 0.197" insert yielded favorable results.

Predominantly, tool failure was isolated to intermittent cutting due to the roundness issues with the motor cases. At the beginning of the cutting cycle, it was not uncommon for the insert to emerge completely out of the kerf and re-engaged at a follow-on point. This intermittent cutting was not very well tolerated by the inserts and was typically the cause of catastrophic tool failure.

To overcome the motor case roundness issues, a device was added to the tool slide that tracks the outer diameter of the motor case (See Figure 4.8). The outer diameter (OD) tracker housed the tool slide and the insert. The OD tracker was a profitable solution to eliminating catastrophic tool failure.

Having successfully demonstrated that the RLS could segment a 4130 steel alloy motor case, the issues and uncertainty associated with the tool and propellant interface still remained. While the thermal profile data gave favorable temperature ranges in the coolant controlled conditions, there were two unsurpassable conditions remaining. The unpredictability of pinch points in removing the wedding band and the propellant contamination from the coolant.

The T-15 tooling was selected primarily for the aluminum motor cases. Good machining practices allows for the majority of the heat generated during chip formation to be taken away with the chip. Tool selection is critical in achieving heat control. The ductility of the aluminum is forgiving and reduces the amount of energy required for chip formation.

The T-15 tooling usually performs at a higher resident temperature. Tool wear is a major element in the life of the tool; however, the T-15 tooling can be re-shaped and reused, extending its overall service life.

Figure 4.15 illustrates chip formation and removal during the segmenting of an aluminum motor case. Because the T-15 holds heat longer and rises higher during machining, its use for machining the 4130 steel alloy is abandoned in lieu of the wedding band removal and contact with the propellant.

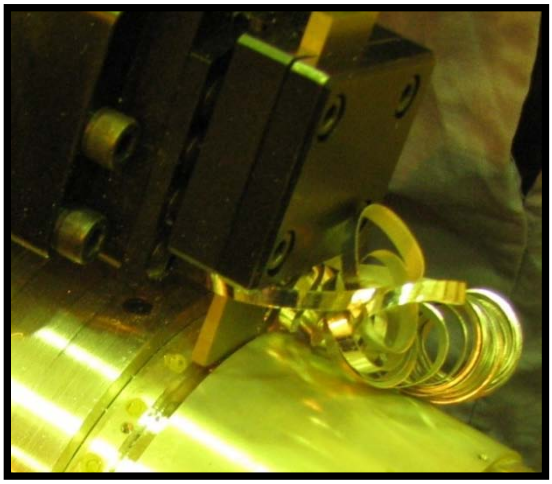

Figure 4.15: T-15 Machining Aluminum.

4.4 Propellant Segmenting

Propellant segmenting, while in itself a separate operation, carries many of the same requirements as the metal removal process. In order for the RMS capability to produce the appropriate through put, the propellant segmenting must function within the same time frame as the metal removal process. The concept for propellant segmenting utilizes similar mechanical devices as the metal cutting operation. Using a patented, omni-directional, diamond impregnated wire saw, many inert tests were successfully demonstrated.

The first series of tests included the radial lathe and a tool set conducive for mounting and applying tension to the two opposing wires. The two wires (0.0276" diameter) were seated in the kerf, loaded in tension (approximately 90 pounds) and

rotated by the radial lathe about the circumference of the rocket motor. This action caused the wires to pass through the propellant and complete the segmenting process.

Critical to this operation is the thermal response. Once again, the IR camera was utilized to collect data on each of the segmenting events and the graphical results are included in Appendix C. Fortunately, the wire saw's unique design has yielded remarkable results for repeatability, surface finish, thermal profile, and cycle time.

Figure 4.16 illustrates the smooth, even surface finish that the wire saw creates. The resultant segmented motor case and exposed propellant condition provides incredible opportunity for numerous downstream propellant processes.

The temperature profile generated during the propellant segmenting was remarkably stable and favorable in a range of 10 to 15 degrees above ambient. Most significant was the cycle time of less than 3 minutes.

Unfortunately, service life for the 0.0276" diameter wire was unfavorable. The pre-load of 90 pounds compounded by the friction load from the propellant caused catastrophic failure. The stress point for failure was near the cable thimble and wire crimp assembly.

In the second series of tests, the compression springs were replaced by pneumatic cylinders. The cylinders were pressurized (90 pounds) by two composite reservoirs installed on the radial lathe. In these tests, the wire saw was doubled in strength. The opposing wires each included 2 wires twisted together to form a rope. This arrangement extended the service life and eliminated the catastrophic failure mode.

While favorable results were obtained with the rope wire saw, an unfavorable condition was created in the crevices of the rope where propellant crumb collected. The

information gathered in this test series was considered successful in that the failure mode was eliminated.

For the third series of tests, a larger wire saw (0.039” diameter) was used in the same system as with test series two. The saw arrangement was the same as the first test series. The pre-load was 140 pounds on the cylinders.

To date, service life continues as a failure mode and has yet to be realized. Indisputably, the 0.039” diameter meets the requirement for thermal profile, surface finish, cycle time, and repeatability.

Additionally, efforts focused on developing minimal segment lengths and time required to complete the segmenting process. Figure 4.16 illustrates one of the successful inert segments. The segment shown in Figure 4.16 is a 3/16” thick segment that was completed in approximately two and a half minutes.

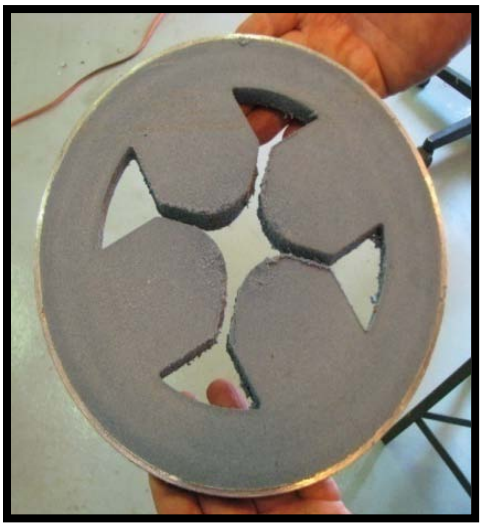

Figure 4.16: Rocket Motor Segment (Inert).

4.5 Half Angle Roller Wheel

The results generated in Section 4.3.1 motivated the requirement to develop a method to remove the wedding band without pinch point issues and introducing or generating excessive heat. This requirement developed the half angle roller wheel (HARW) tooling for the kerf formation step. Figure 4.17 illustrates the tooling profile.

Figure 4.17: Half Angle Roller Wheel.

The segmenting process starts with the metal removal process stopping just short of completing the full depth of cut. This approach leaves approximately 0.030" of metal in the bottom of the kerf which was enough to give the remaining metal memory or plasticity.

As the HARW was driven past the kerf and into the propellant, the kerf was cold rolled and curled down against one side of the kerf wall. The results fit remarkably well for kerf formation and preparation of the propellant segmenting process.

Several HARW profiles were tested and included attack angles from 22.5^{o} to 45^{o}. Ultimately, the 35^{o} HARW formed the most suitable kerf for propellant segmenting and is illustrated in Figure 4.18. Because the load on the HARW was minimized by the thin

layer of metal in the bottom of the kerf, very little energy was put into the process which keeps the temperature near ambient.

Figure 4.18: HARW and Kerf Formation

4.6 Analytical Results

In developing the RMS technology, the primary and critical element was temperature control between the segmenting process and the interface with the propellant. The motivation within this effort was to design and develop a technique for metal removal without exciting the propellant. The one constant operational parameter was to the thermal response of the cutting operations below the auto-ignition temperature of the propellant.

Other issues included point points and coolant contamination. The LMS insert tests established a repeatable range of temperatures that was below the auto-ignition temperature of the propellant. Using Equation 3.8, and this temperature data, an approximation for cutting force, F_c can be determined.

Appendix C contains the mathematical model for solving for a range of the temperature using the cutting force. Using an iterative approach for cutting force values, a range of solutions for Equation 3.8 can be calculated.

Changing the values for cutting force until the solutions for Equation 3.8 match the thermal profile generated during the RLS insert test will establish a range of forces being applied to the system. The cutting force data can then be inputs for determining the analytical approximation for the induced stresses in the RWS process. Appendix D contains the mathematical model for the RWS analysis.

Chapter 5

CONCLUSION

The purpose of this research was to investigate existing technologies suitable for integration into and development of a rocket motor segmenting capability. Within the scope of this effort were the responsibilities of meeting the requirements for safety, efficiency, and throughput rates to satisfy the impending demil workload for rocket motor propellant removal.

The RMS design considerations were challenged by the requirement of being an elemental function within the big picture of a site plan for missile system processing. The RMS footprint will include conveyance for receiving and loading the rocket motors into the system and also providing feedstock to the downstream functions for propellant processing at a minimum rate of one motor every 15 minutes.

The path to the development of an RMS has included utilization of COTS technology and equipment which fulfills one of the many overarching requirements. The research and development has provided sound data, physical evidence, and suitable technologies for developing the RMS process.

The current efforts have validated two technologies regarding the down selection decision matrix that have potential for maturation into a deployable capability for RMS. The WJS is a mature technology but requires integration into an RMS capability. The path forward for the RLS operations is being refined to develop a prototype segmenting station capable of providing a safe and economical footprint that meets a required throughput in support of potential downstream feedstock demands. Both capabilities will

be evaluated for final technology down selection and deployment post maturation of the RLS.

A tremendous effort was expended on the RWS because of the possibility of eliminating chips and coolant. While the RWS concept was proven, inherent to the process was the elasticity of the MLRS propellant causing the kerf to close up after the segmentation event. While this condition eliminated the MLRS rocket motor as a candidate, other rocket motors with more ductile casings have the potential of being feedstock for the RWS technique.

The purpose of conducting the RLS tests without coolant is to develop a temperature profile of the worst case scenario. If the downstream process of removing the propellant from the segmented motor case prohibits inclusions that contaminate the original chemistry of the propellant, then the RMS is restricted from coolants.

Due to the nature of the cutting action of the wire saw, small propellant particles (crumb) as were to be expected, generated the requirement for a wet-vacuum particle collection system as a part of the overall RMS footprint. Research is underway to design, fabricate, and demonstrate the wet-vacuum particle collection system. The intent continues with the theme of the RMS of selecting a COTS item and modifying it to meet the RMS needs. Summarizing, the RMS requirements indicate that the segmenting system cannot contaminate the propellant with coolant, must maintain a predictable thermal profile, collect dust and crumb particles in the wire sawing event, and finally meet a throughput rate conducive to the flow of the entire missile system demil site process.

Combining the RLS techniques has created the three phase RMS system. Phase one is the metal removal portion. Phase two is the kerf formation process. Phase three is the propellant segmenting process. Each phase has a unique process and tooling.

Phase one uses inserts to remove the metal and develop a kerf. Phase two uses the HARW tooling to form the kerf and expose the propellant. Phase three uses the wire saw to segment the propellant.

The RMS will process one motor every 12 minutes including receiving the motor into the system and delivering the segmented motor sections to the downstream processes. The current estimate developed during the sub-scale demonstrations is 14.2 minutes per MLRS motor.

Appendix D includes a 3-dimensional concept drawing of the prototype RMS incorporating the three phase RMS techniques. The prototype RMS development is well underway and on schedule for installation and demonstration at the RSA in July of 2010.

APPENDIX A

Thermal Graphs

For

RLS Insert Demonstrations

And

Thermal Profiling

Red Line = Temperature in the kerf (Critical Data)

Green Line = Average of kerf and ambient

Blue Line = Ambient Temperature

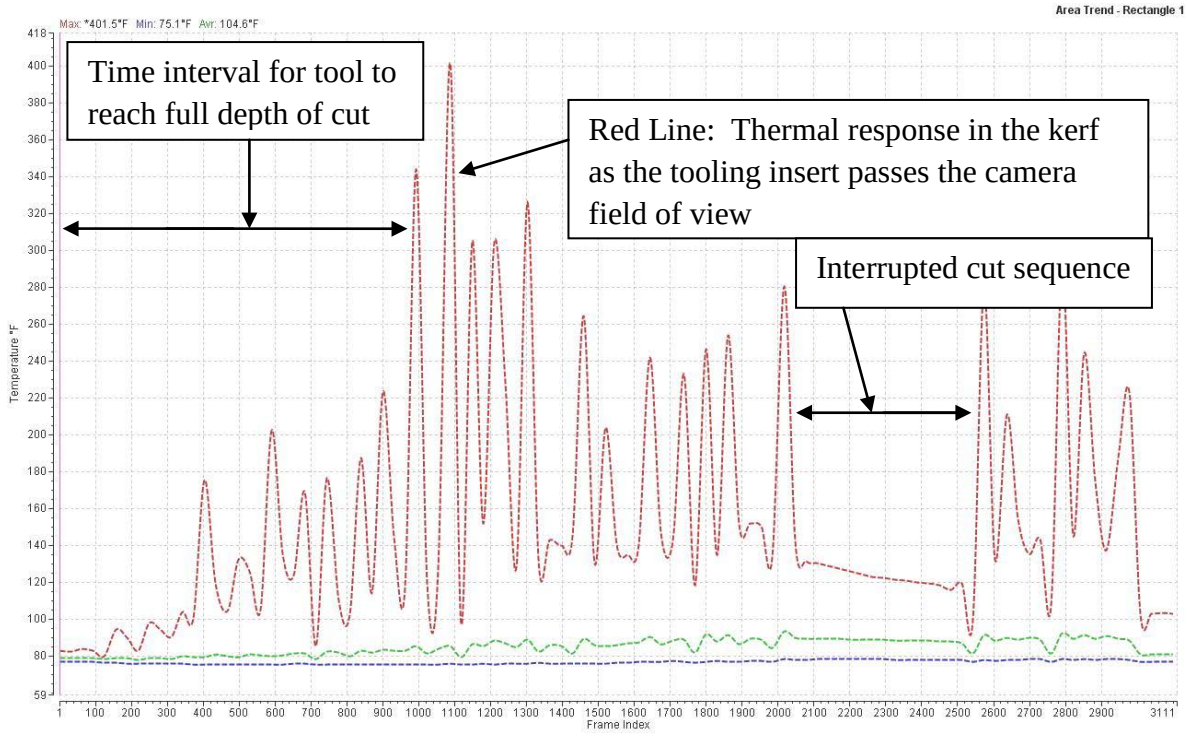
Area Trend - Rectangle 1
Max: *401.5*F Min: 75.1*F Avr: 104.6*F
Time interval for tool to reach full depth of cut
Red Line: Thermal response in the kerf as the tooling insert passes the camera field of view
Interrupted cut sequence
Temperature *F
Frame Index

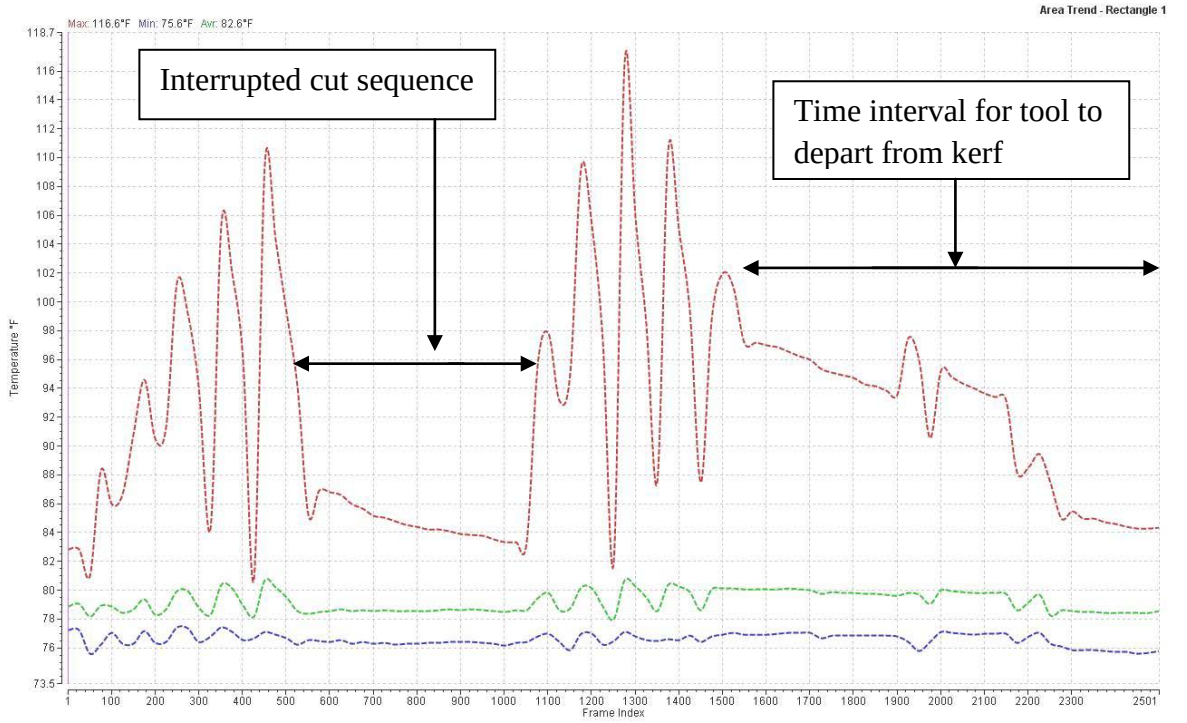
Area Trend - Rectangle 1
Max: 116.6*F Min: 75.6*F Avr: 82.6*F
Interrupted cut sequence
Time interval for tool to depart from kerf
Temperature *F
Frame Index

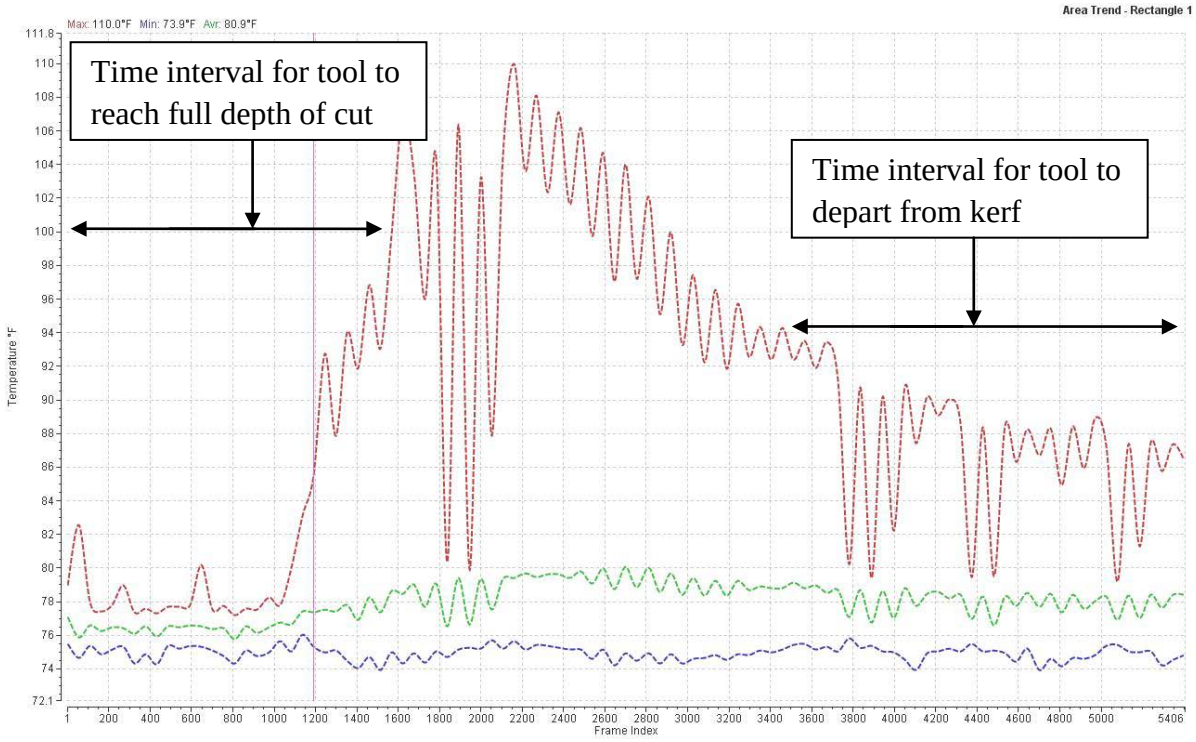
Area Trend - Rectangle 1
Max: 110.0°F Min: 73.9°F Avr: 80.9°F
Time interval for tool to reach full depth of cut
Time interval for tool to depart from kerf
Temperature °F
Frame Index


Area Trend - Rectangle 1
Max: 159.4°F Min: 74.2°F Avr: 90.0°F
Temperature °F
Frame Index

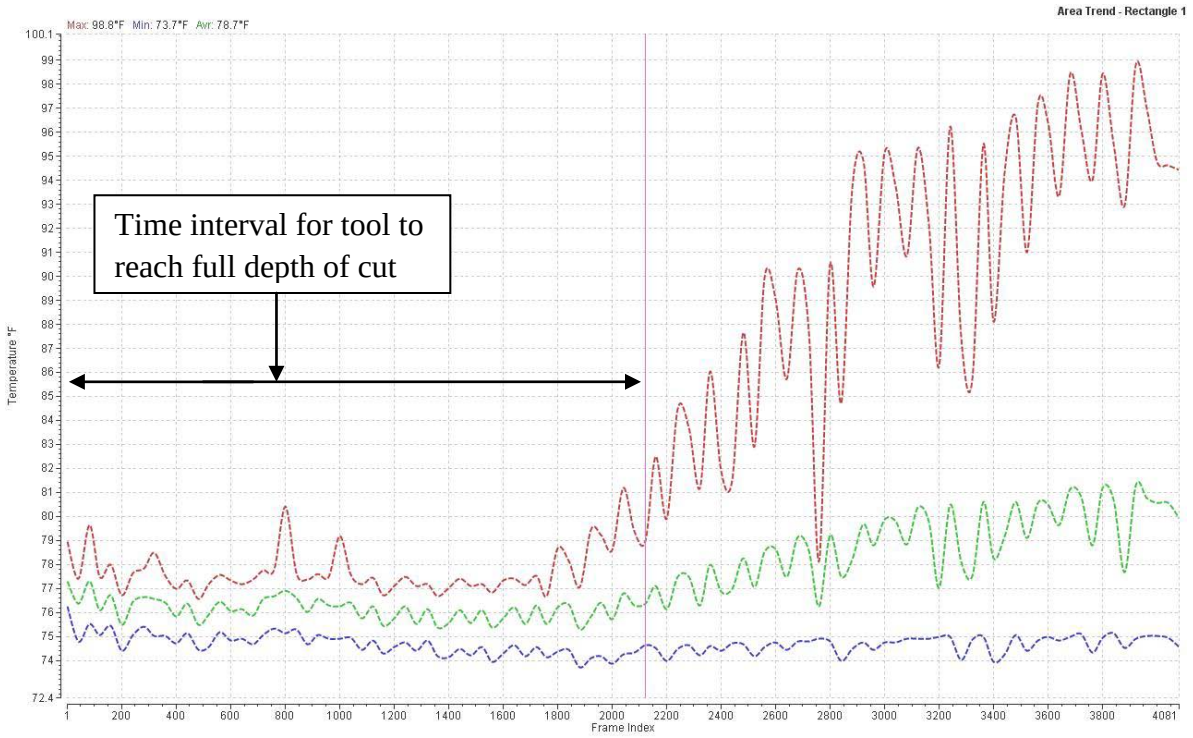
Area Trend - Rectangle 1
Max: 98.8°F Min: 73.7°F Avr: 78.7°F
Time interval for tool to reach full depth of cut
Temperature °F
Frame Index

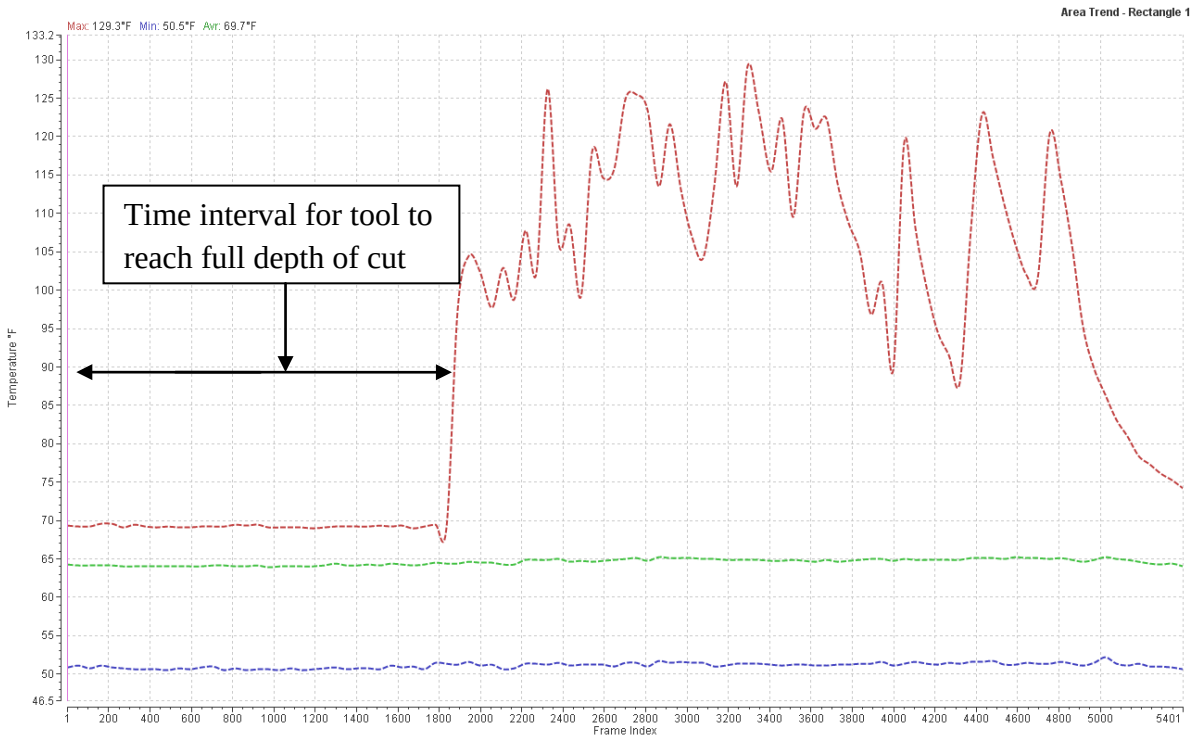
Area Trend - Rectangle 1
Max: 129.3°F Min: 50.5°F Avr: 69.7°F
Time interval for tool to reach full depth of cut
Temperature °F
Frame Index

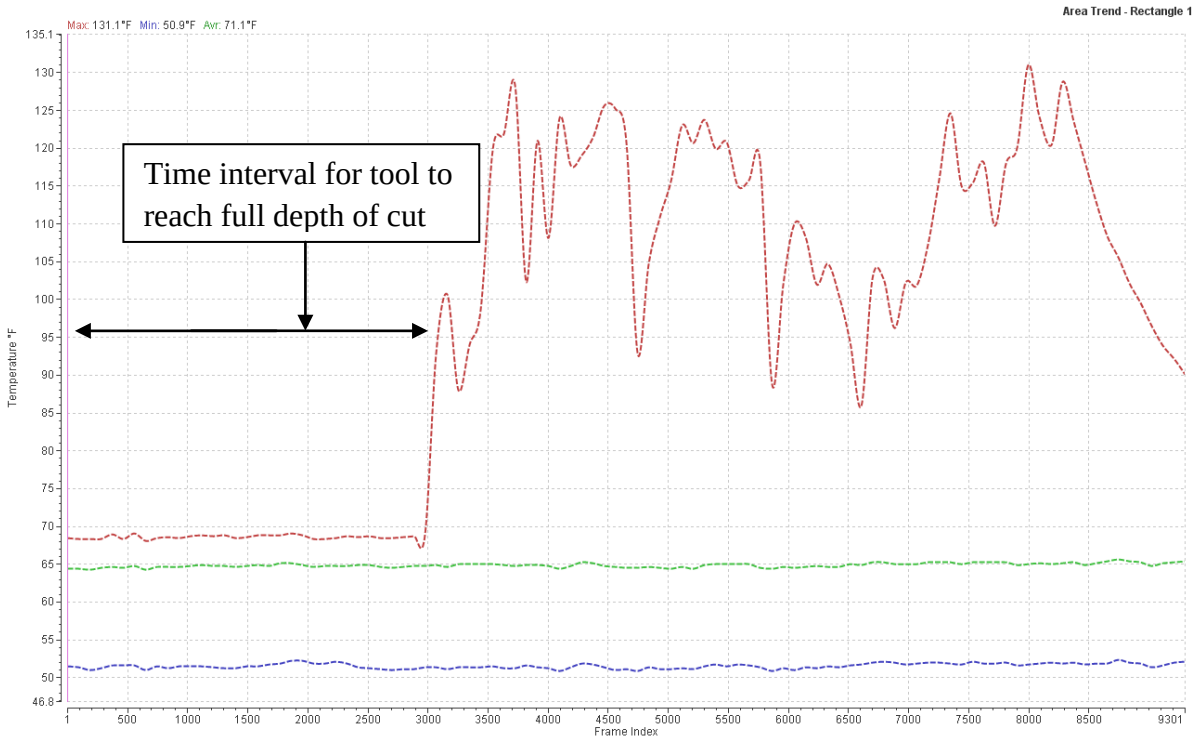
Area Trend - Rectangle 1
Max: 131.1°F Min: 50.9°F Avr: 71.1°F
Time interval for tool to reach full depth of cut
Temperature °F
Frame Index

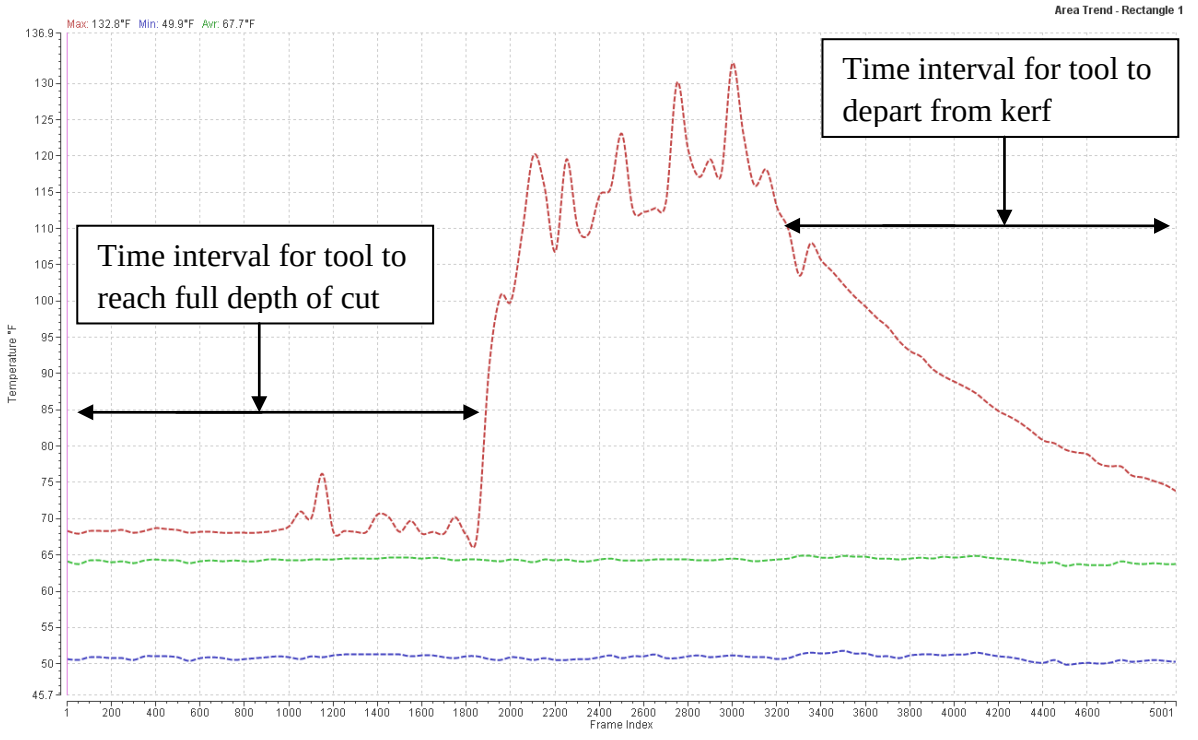
Area Trend - Rectangle 1
Max: 132.8°F Min: 49.9°F Avr: 67.7°F
Time interval for tool to depart from kerf
Time interval for tool to reach full depth of cut
Temperature °F
Frame Index

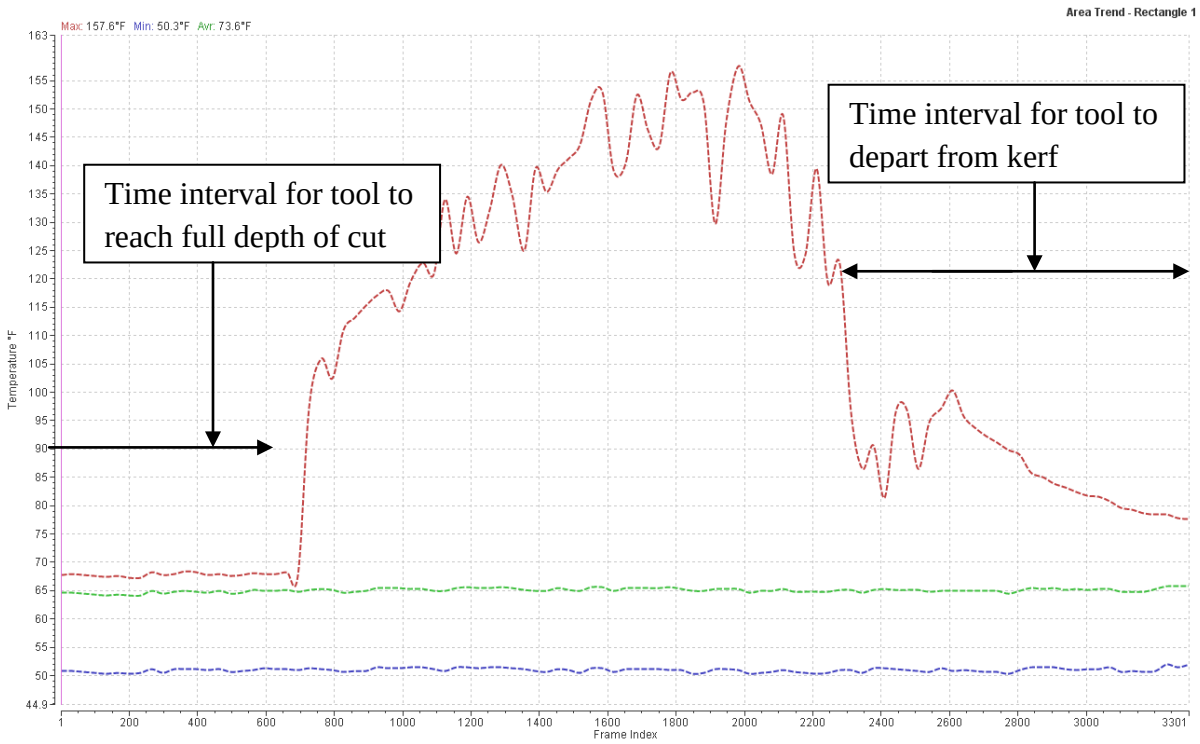
Area Trend - Rectangle 1
Max: 157.6°F Min: 50.3°F Avr: 73.6°F
Temperature °F
Frame Index
Time interval for tool to reach full depth of cut
Time interval for tool to depart from kerf

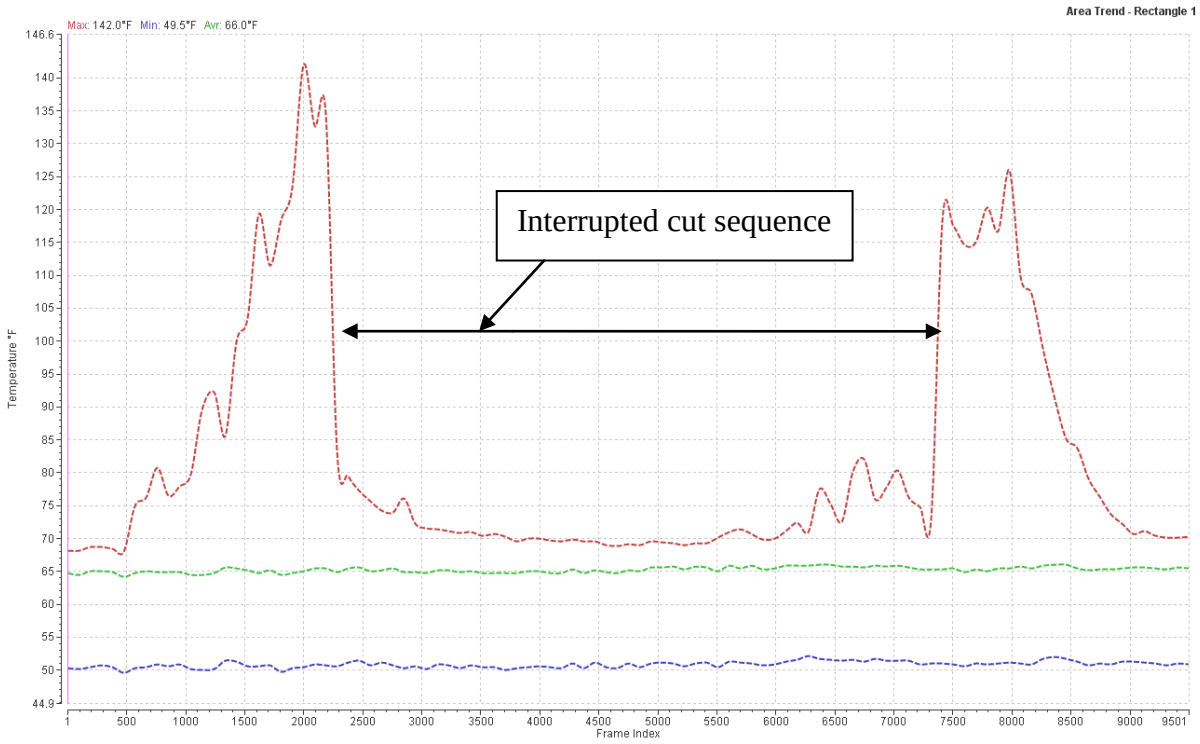
Area Trend - Rectangle 1
Max: 142.0°F Min: 49.5°F Avr: 66.0°F
Temperature °F
Frame Index
Interrupted cut sequence

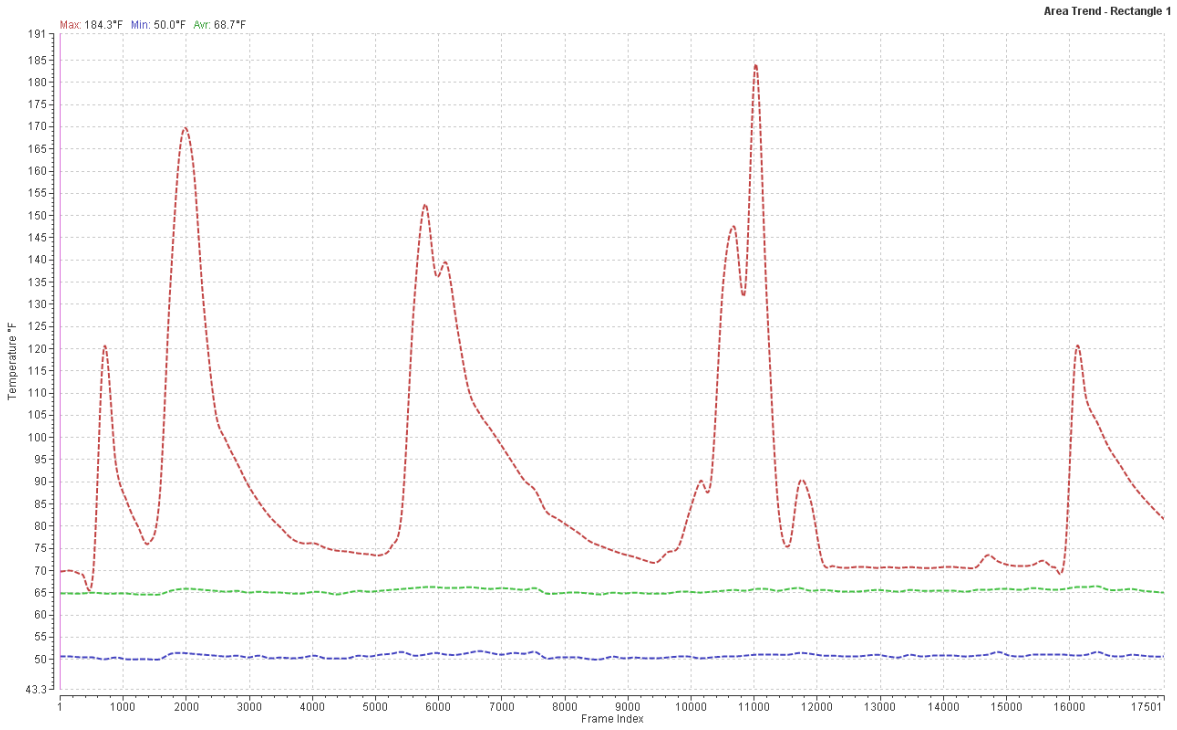

Mid stream time stamp of kerf temperature

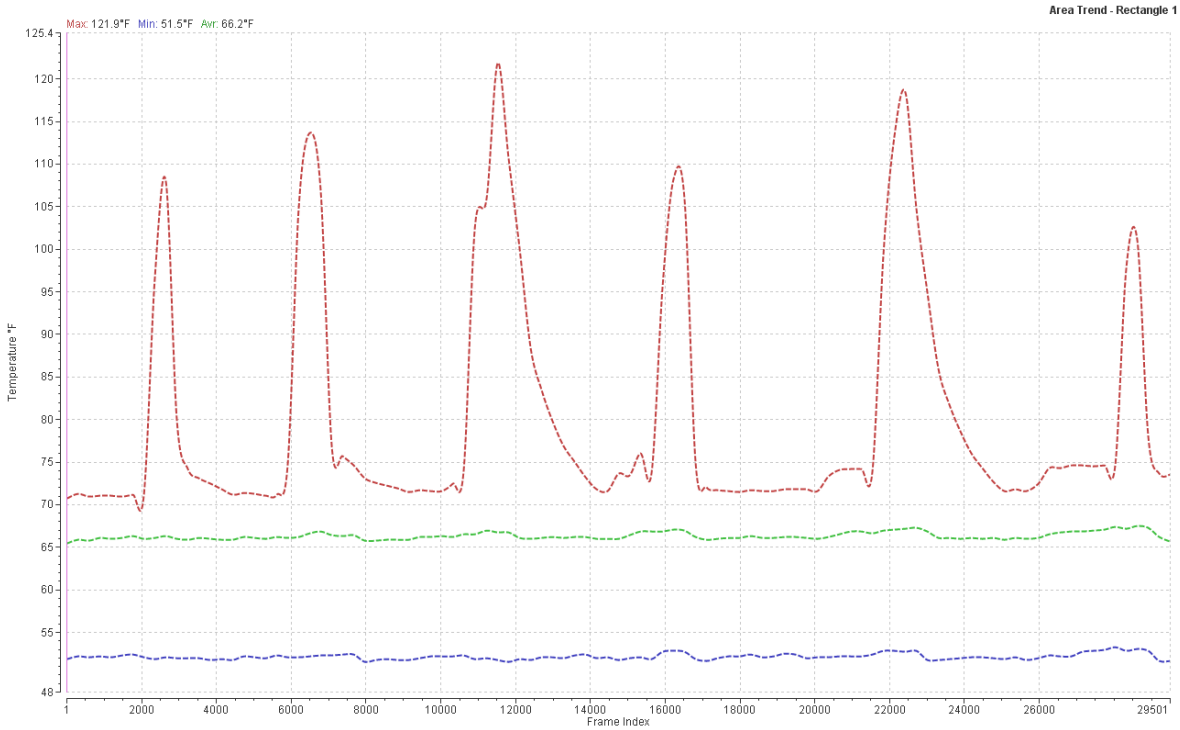

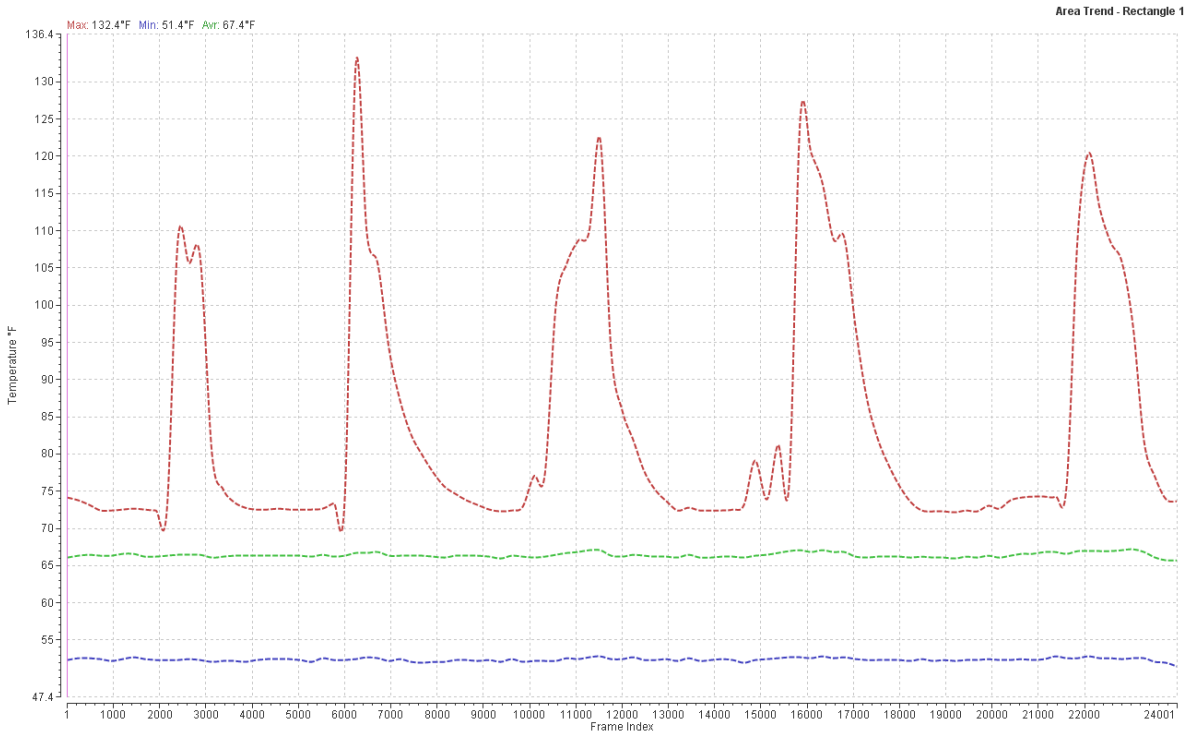

Mid stream time stamp of kerf temperature

APPENDIX B

Graphical Data

For

Coolant Analysis

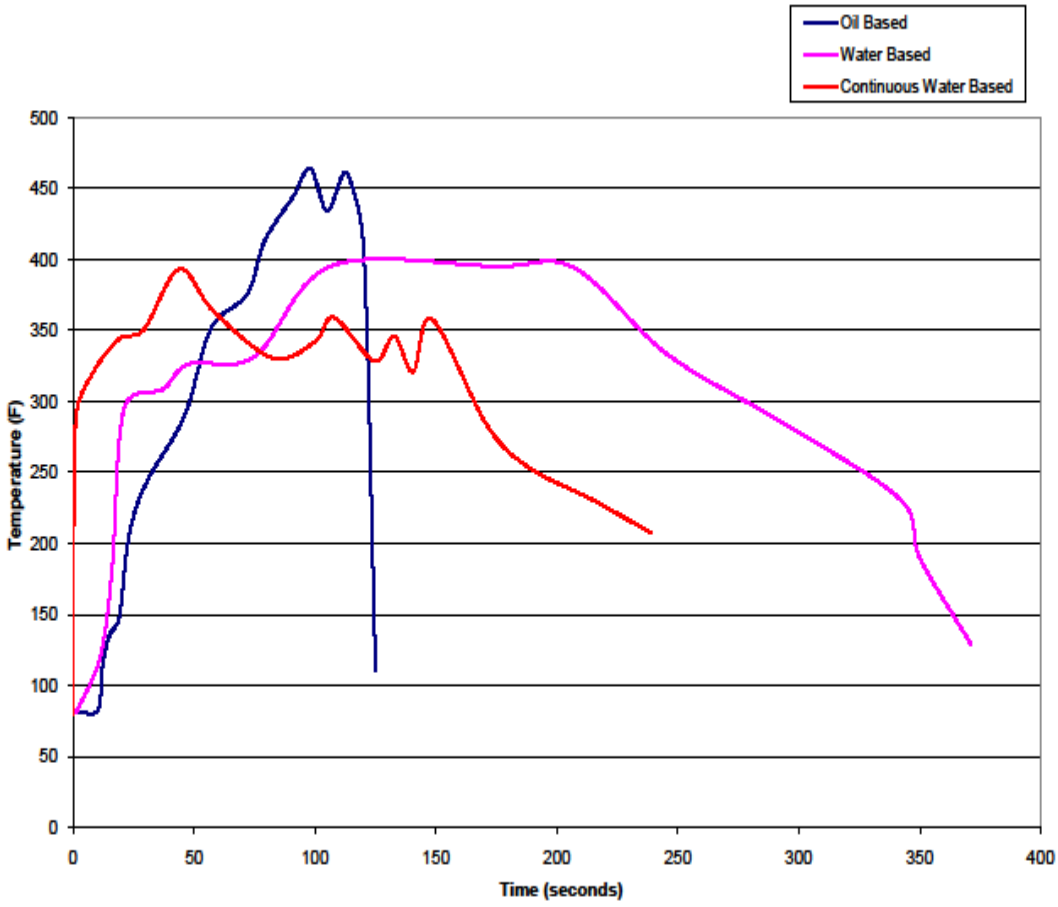

Figure B.1: Representative Data for Temperature Profile from Various Coolants.

Graph of the kerf thermal response using various coolant types. Continuous water based coolant provided optimum temperature profile.

APPENDIX C

Thermal Images

For

Temperature Profile

Of

Propellant Segmenting

Images validate that the temperature profile for propellant cutting is 10 to 20 degrees above ambient (10^{o} C – 20^{o} C).

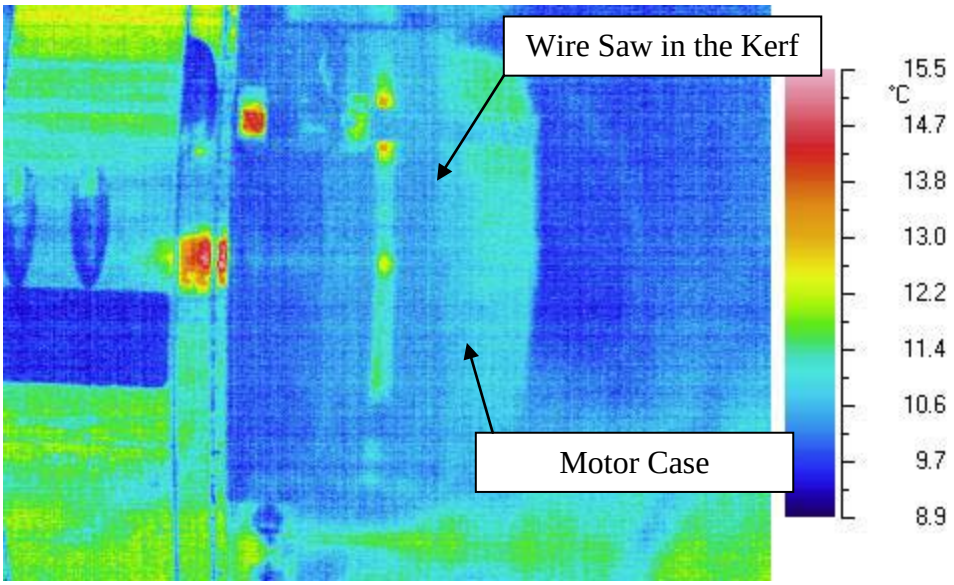
Wire Saw in the Kerf
Motor Case
15.5
°C
14.7
13.8
13.0
12.2
11.4
10.6
9.7
8.9

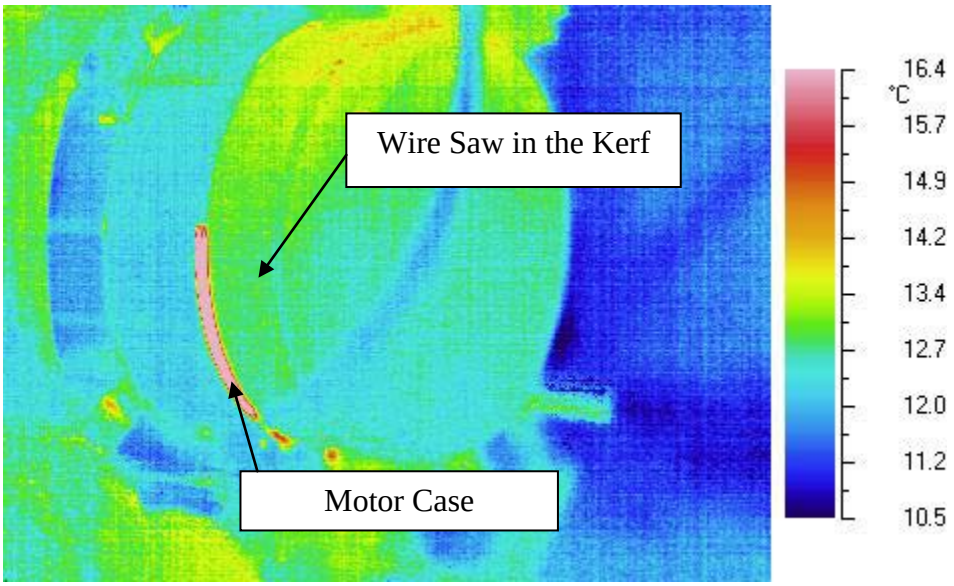
Wire Saw in the Kerf
Motor Case
16.4
°C
15.7
14.9
14.2
13.4
12.7
12.0
11.2
10.5

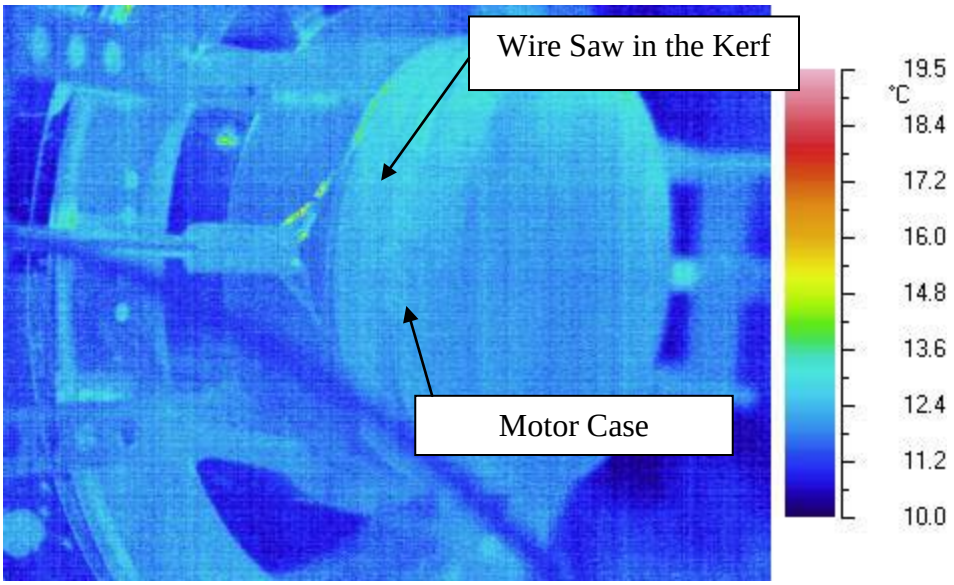
Wire Saw in the Kerf
Motor Case
19.5
°C
18.4
17.2
16.0
14.8
13.6
12.4
11.2
10.0

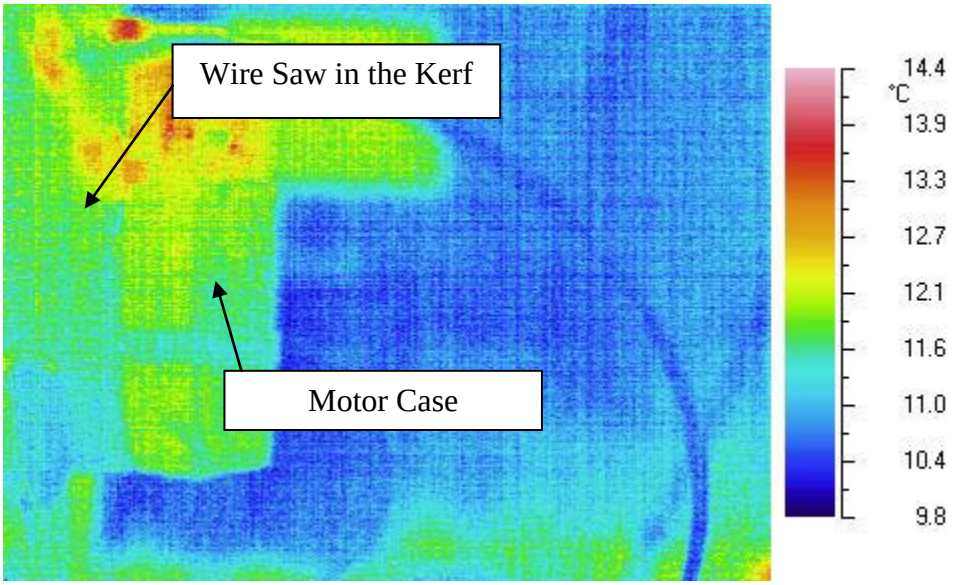
Wire Saw in the Kerf
Motor Case
14.4
°C
13.9
13.3
12.7
12.1
11.6
11.0
10.4
9.8

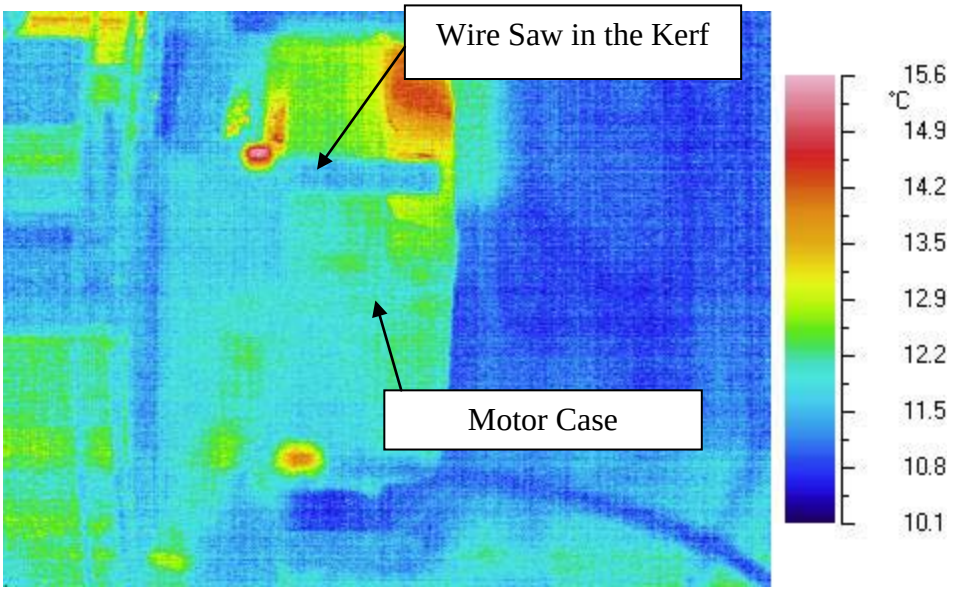
Wire Saw in the Kerf
Motor Case
15.6
°C
14.9
14.2
13.5
12.9
12.2
11.5
10.8
10.1

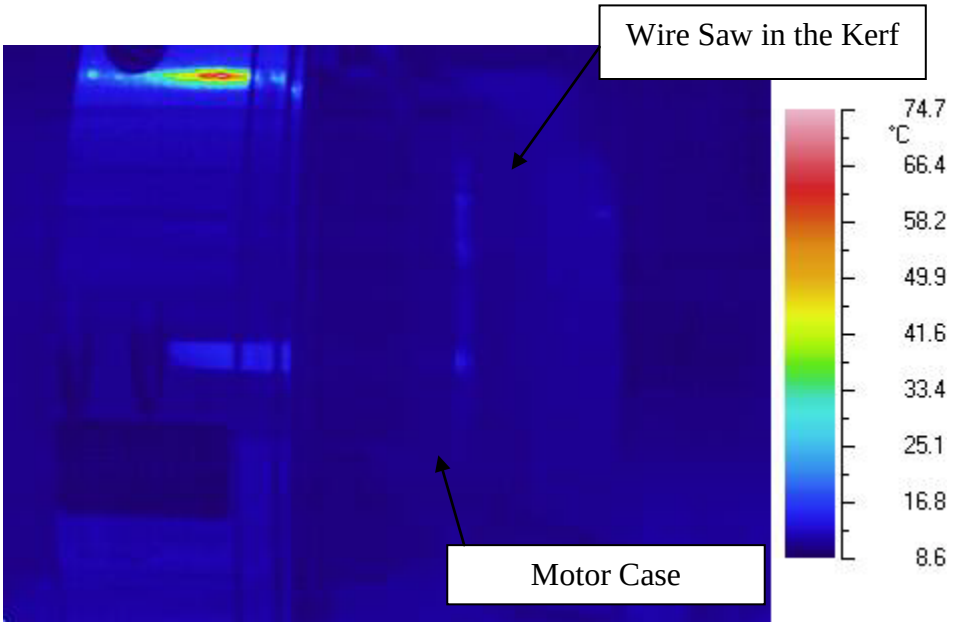
Wire Saw in the Kerf
Motor Case
74.7
°C
66.4
58.2
49.9
41.6
33.4
25.1
16.8
8.6

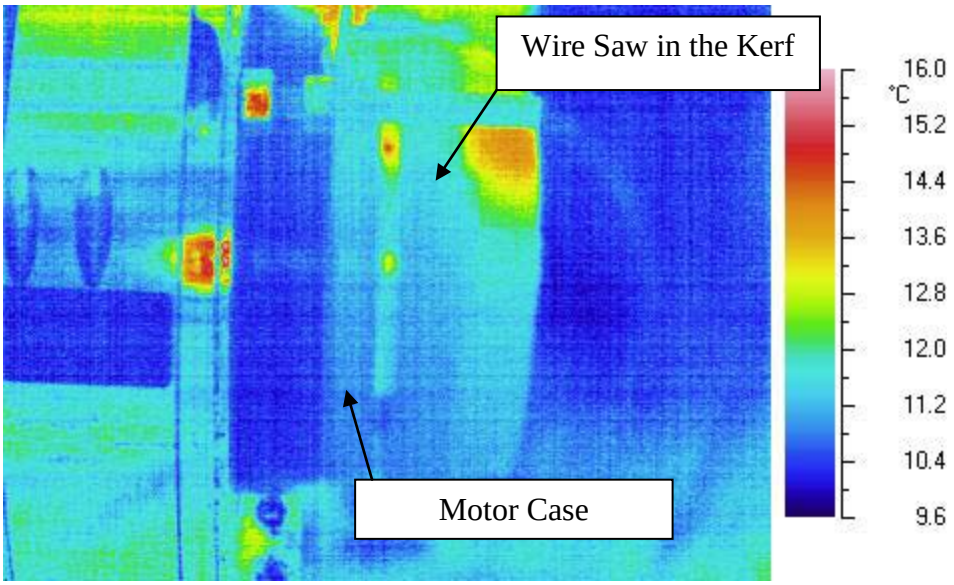
Wire Saw in the Kerf
Motor Case
16.0
°C
15.2
14.4
13.6
12.8
12.0
11.2
10.4
9.6

APPENDIX D

Analytical Results

D1 is outer diameter of work piece
D2 is outer diameter after metal removal
d = DOC
Ve = speed in surface feet per minute
Ns = revolutions per minute
fr = feed rate
r = radius
Le = distance of cut
allow = lead time before and
after tool interface w/ material
le = length of the chip
ρ = density of the steel
SH = specific heat
Vc = chip velocity
Vs = shear velocity
Lc =chip contact with rake face
w = width of tooling
wc = weight of the chip
w1 = unformed chip thickness
t1 = uncut chip thickness = fr
t2 = cut chip thickness
α = back rake angle
ϕ = shear plane angle
ψ = shear lamella

RF = resultant force acting on the back of the chip
R' = resultant force acting on the shear plane
Ffr = friction force
NF = normal force acting on the tool/chip interface
Fs = shear force acting on the shear plane
Fn = normal force acting on the shear plane area
As = shear plane area
Fc = cutting force
Ft = tangential (normal force)
β = friction angle
μ = friction coefficient on tool/chip interface area
τ = shear stress
τs = shear stress (flow stress)
E = efficiency of the machine
β1= Boothroyd's experimental curve for the proportion of heat conducted back into the work material
b = width of the contact
a = length of the contact

Iterative approach for determining cutting forces based on actual temperature profile:

$D_1 := 8.97 \cdot in$ $D_2 := 8.65 \cdot in$ $le := 0.8 \cdot in$

$\rho := 0.284 \cdot \frac{lb}{in^3}$ $N_s := 18 \cdot rpm$ $N_s = 0.3 \frac{rev}{sec}$ $w1 := 0.197 \cdot in$

$allow := 5$

$f_r := .0044 \cdot \frac{in}{rev}$ $SH := 0.114 \cdot \frac{BTU}{lb \cdot F}$ $r := \frac{D_1}{2}$

$d := \frac{D_1 - D_2}{2}$ $d = 0.16\,in$ $V_e := \frac{\pi \cdot D_1 \cdot N_s}{12}$ $V_e = 4.427 \frac{in}{sec}$

$L_e := revo \cdot 2 \cdot \pi \cdot r$ $L_e = 1024.73\,in$

$\phi := 28 \cdot deg$ $kt := 42.7 \cdot \frac{W}{m \cdot K}$

$t_1 := 0.0044 \cdot in$ $\alpha := 9 \cdot deg$

$w := .197 \cdot in$ $wc := .0063305 \cdot oz$

$t_2 := \frac{wc}{\rho \cdot w1 \cdot le}$ $t_2 = 0.009\,in$

$V_s := V_e \cdot \left(\frac{\cos(\phi)}{\cos(\phi - \alpha)} \right)$ $V_c := V_e \cdot r_c$

$V_s = 4.134 \frac{in}{sec}$ $V_c = 2.198 \frac{in}{sec}$

$$F_c := \begin{pmatrix} 150 \\ 175 \\ 200 \\ 225 \\ 250 \\ 275 \\ 300 \\ 325 \\ 350 \\ 375 \end{pmatrix} \cdot lbf \qquad \begin{pmatrix} 30 \\ 40 \\ 50 \\ 60 \\ 70 \\ 80 \\ 90 \\ 100 \\ 110 \\ 120 \end{pmatrix} \begin{pmatrix} 50 \\ 75 \\ 100 \\ 125 \\ 150 \\ 175 \\ 200 \\ 225 \\ 250 \\ 275 \end{pmatrix} \begin{pmatrix} 100 \\ 125 \\ 150 \\ 175 \\ 200 \\ 225 \\ 250 \\ 275 \\ 300 \\ 325 \end{pmatrix} \begin{pmatrix} 150 \\ 175 \\ 200 \\ 225 \\ 250 \\ 275 \\ 300 \\ 325 \\ 350 \\ 375 \end{pmatrix} \begin{pmatrix} 200 \\ 225 \\ 250 \\ 275 \\ 300 \\ 325 \\ 350 \\ 375 \\ 400 \\ 425 \end{pmatrix} \begin{pmatrix} 200 \\ 205 \\ 210 \\ 215 \\ 220 \\ 225 \\ 230 \\ 235 \\ 240 \\ 245 \end{pmatrix} \begin{pmatrix} 300 \\ 325 \\ 350 \\ 375 \\ 400 \\ 425 \\ 450 \\ 475 \\ 500 \\ 525 \end{pmatrix}$$

$F_t := .75 \cdot F_c$ $\quad F_t =$

	0
0	112.5
1	131.25
2	150
3	168.75
4	187.5
5	206.25
6	225
7	243.75
8	262.5
9	281.25

lbf

$$(\theta) := \left(\frac{r_c \cdot \cos(\alpha)}{1 - r_c \cdot \sin(\alpha)} \right)$$

$\tan(\theta) = 33.702\,deg$

$N_F := F_c \cdot \cos(\alpha) - F_t \cdot \sin(\alpha)$ $\qquad F_{fr} := F_c \cdot \sin(\alpha) + F_t \cdot \cos(\alpha)$ $\qquad F_s := F_c \cdot \cos(\phi) - F_t \cdot \sin(\phi)$

$\beta := \dfrac{F_{fr}}{N_F}$ $\qquad R_F := \sqrt{F_c^{\,2} + F_t^{\,2}}$

$A_s := \dfrac{t_1 \cdot w}{\sin(\phi)}$

$F_n := F_c \cdot \sin(\phi) - F_t \cdot \cos(\phi)$

$\tau := \dfrac{F_s}{A_s}$ $\qquad A_s = 1.282 \times 10^{-5}\,ft^2$

$$\tau_s := \frac{F_c \cdot \sin(\phi) \cdot \cos(\phi) - F_t \cdot \sin(\phi) \cdot \sin(\phi)}{t_1 \cdot w}$$

$N_F =$

	0
0	130.554
1	152.313
2	174.072
3	195.832
4	217.591
5	239.35
6	261.109
7	282.868
8	304.627
9	326.386

lbf

$R_F =$

	0
0	187.5
1	218.75
2	250
3	281.25
4	312.5
5	343.75
6	375
7	406.25
8	437.5
9	468.75

lbf

$F_{fr} =$

	0
0	134.58
1	157.01
2	179.44
3	201.87
4	224.3
5	246.73
6	269.16
7	291.59
8	314.02
9	336.45

lbf

$\beta =$

	0
0	59.063
1	59.063
2	59.063
3	59.063
4	59.063
5	59.063
6	59.063
7	59.063
8	59.063
9	59.063

deg

$\beta 1 := 0.28$

$$\Delta T := \left[\frac{\left(F_c \cdot \cos(\phi) - F_{fr} \cdot \sin(\phi)\right) \cdot \cos(\alpha)}{\rho \cdot SH \cdot w1 \cdot t_1 \cdot \cos(\phi - \alpha)}\right] \cdot (1 - \beta 1)$$

$\Delta T =$

	0
0	198.779
1	231.909
2	265.039
3	298.169
4	331.299
5	364.429
6	397.559
7	430.689
8	463.818
9	496.948

F

$F_n =$

	0
0	-28.911
1	-33.729
2	-38.548
3	-43.366
4	-48.185
5	-53.003
6	-57.822
7	-62.64
8	-67.459
9	-72.277

lbf

$F_s =$

	0
0	79.627
1	92.898
2	106.169
3	119.44
4	132.711
5	145.982
6	159.253
7	172.524
8	185.795
9	199.066

lbf

$\tau_s =$

	0
0	$4.313 \cdot 10^4$
1	$5.031 \cdot 10^4$
2	$5.75 \cdot 10^4$
3	$6.469 \cdot 10^4$
4	$7.188 \cdot 10^4$
5	$7.907 \cdot 10^4$
6	$8.625 \cdot 10^4$
7	$9.344 \cdot 10^4$
8	$1.006 \cdot 10^5$
9	$1.078 \cdot 10^5$

psi

$\tau =$

	0
0	$4.313 \cdot 10^4$
1	$5.031 \cdot 10^4$
2	$5.75 \cdot 10^4$
3	$6.469 \cdot 10^4$
4	$7.188 \cdot 10^4$
5	$7.907 \cdot 10^4$
6	$8.625 \cdot 10^4$
7	$9.344 \cdot 10^4$
8	$1.006 \cdot 10^5$
9	$1.078 \cdot 10^5$

psi

ORIGIN := 1

M := 10

i := 1.. M

$F_c := \begin{pmatrix} 150 \\ 175 \\ 200 \\ 225 \\ 250 \\ 275 \\ 300 \\ 325 \\ 350 \\ 375 \end{pmatrix} \cdot lbf$

$P := \frac{F_c}{z}$

$\theta := 10$

$x_r := .02in$

$z := .02in$

$\alpha := 10$

$L := .01 \cdot in$

$r := \frac{x_r}{\cos(\theta)}$

$\sigma_r := \frac{-P \cdot \cos(\theta)}{r \cdot \left(\alpha + \frac{1}{2} \cdot \sin(2 \cdot \alpha) \right)}$

$\sigma_r =$ psi

	1
1	-3·10 4
2	-3·10 4
3	-3·10 4
4	-4·10 4
5	-4·10 4
6	-5·10 4
7	-5·10 4
8	-5·10 4
9	-6·10 4
10	-6·10 4

$\sigma_x := \frac{-P \cdot \cos(\theta)^4}{L \cdot \left(\alpha + \frac{1}{2} \cdot \sin(2 \cdot \alpha) \right)}$

$\sigma_x =$ psi

	1
1	-4·10 4
2	-4·10 4
3	-5·10 4
4	-5·10 4
5	-6·10 4
6	-7·10 4
7	-7·10 4
8	-8·10 4
9	-8·10 4
10	-9·10 4

$\Delta\sigma_x := \frac{-P \cdot \left(1 - \cos(\alpha)^4\right)}{L \cdot \left(\alpha + \frac{1}{2} \cdot \sin(2 \cdot \alpha) \right)}$

$\Delta\sigma_x =$ psi

	1
1	-4·10 4
2	-4·10 4
3	-5·10 4
4	-5·10 4
5	-6·10 4
6	-7·10 4
7	-7·10 4
8	-8·10 4
9	-8·10 4
10	-9·10 4

$P =$ $\frac{lbf}{in}$

	1
1	8·10 3
2	9·10 3
3	1·10 4
4	1·10 4
5	1·10 4
6	1·10 4
7	2·10 4
8	2·10 4
9	2·10 4
10	2·10 4

Maximum Stresses:

$\nu_1 := 0.3$ $\quad E_1 := 29500000 \cdot psi$ $\quad d_1 := 1.95 \cdot in$

$\nu_2 := 0.3$ $\quad E_2 := 30460000 \cdot psi$ $\quad d_2 := 8.97 \cdot in$

$le := .02 \cdot in$

$$P := \begin{pmatrix} 188 \\ 219 \\ 250 \\ 281 \\ 313 \\ 344 \\ 375 \\ 406 \\ 438 \\ 469 \end{pmatrix} \cdot lbf \qquad r_1 := \frac{d_1}{2} \qquad r_2 := \frac{d_2}{2}$$

$$Ka := \left(\frac{\frac{1-\nu_1^2}{E_1} + \frac{1-\nu_2^2}{E_2}}{\frac{1}{d_1} + \frac{1}{d_2}} \right)^{\frac{1}{3}}$$

$$a := Ka \cdot P^{\frac{1}{3}} \qquad b := \left[\frac{4 \cdot P \cdot r_1 \cdot r_2}{\pi \cdot le \cdot (r_1 + r_2)} \cdot \left(\frac{1-\nu_1^2}{E_1} + \frac{1-\nu_2^2}{E_2} \right) \right]^{\frac{1}{2}}$$

$$\sigma max := \frac{2 \cdot P}{\pi \cdot b \cdot a}$$

$\sigma max =$

	0
0	$1 \cdot 10^4$
1	$1 \cdot 10^4$
2	$2 \cdot 10^4$
3	$2 \cdot 10^4$
4	$2 \cdot 10^4$
5	$2 \cdot 10^4$
6	$2 \cdot 10^4$
7	$3 \cdot 10^4$
8	$3 \cdot 10^4$
9	$3 \cdot 10^4$

psi

$b =$

	0
0	0.024
1	0.026
2	0.028
3	0.029
4	0.031
5	0.033
6	0.034
7	0.035
8	0.037
9	0.038

in

$a =$

	0
0	0.026
1	0.028
2	0.029
3	0.03
4	0.031
5	0.032
6	0.033
7	0.034
8	0.035
9	0.036

in

Cantilever load:

$\sigma_x := \sigma_r \cdot \cos(\theta)^2$ $\sigma_y := \sigma_r \cdot \sin(\theta)^2$ $\tau := \sigma_r \cdot \sin(\theta) \cdot \cos(\theta)$

$\sigma_x =$

	1
1	-2·10 4
2	-2·10 4
3	-2·10 4
4	-3·10 4
5	-3·10 4
6	-3·10 4
7	-4·10 4
8	-4·10 4
9	-4·10 4
10	-4·10 4

psi

$\sigma_y =$

	1
1	-7.473·10 3
2	-8.718·10 3
3	-9.964·10 3
4	-1.121·10 4
5	-1.245·10 4
6	-1.37·10 4
7	-1.495·10 4
8	-1.619·10 4
9	-1.744·10 4
10	-1.868·10 4

psi

$\tau =$

	1
1	-1·10 4
2	-1·10 4
3	-2·10 4
4	-2·10 4
5	-2·10 4
6	-2·10 4
7	-2·10 4
8	-2·10 4
9	-3·10 4
10	-3·10 4

psi

APPENDIX E

3-D

Of

Prototype RMS

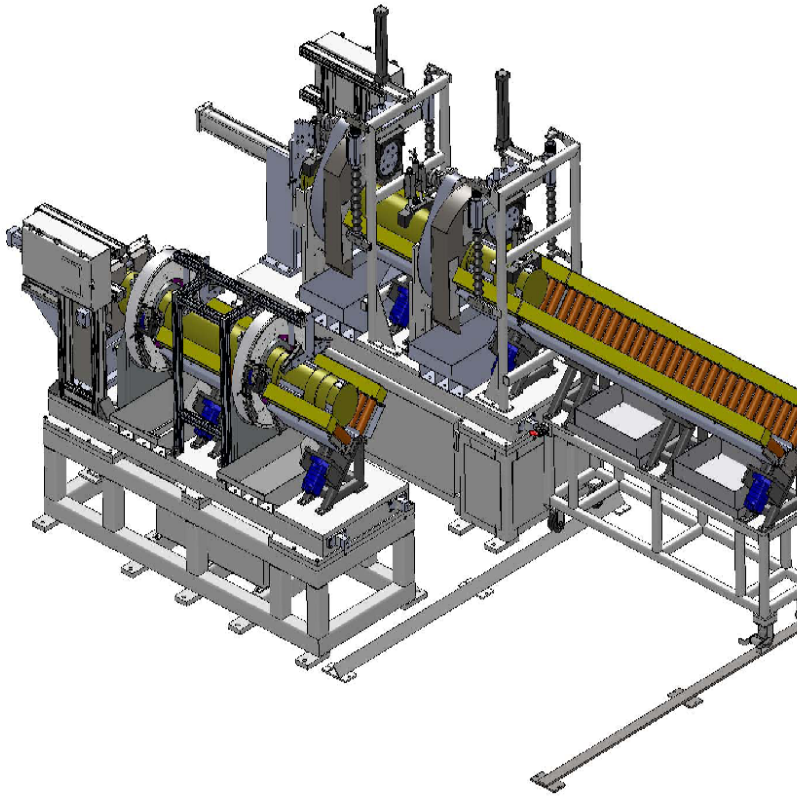

APPENDIX F

List of Acronyms

ANSI	American National Standard Institute
COTS	Commercial-Off-The-Shelf
HARW	Half Angle Roller Wheel
IR	Inferred
LSR	Lathe Stabilizer Ring
MLRS	Multiple Launch Rocket System
OD	Outer Diameter
OSM	Other Service Missiles
PM Demil	Product Manager for Demilitarization
Rc	Rockwell C
RLS	Radial Lathe Segmenting
RMS	Rocket Motor Segmenting
RPM	Revolution Per Minute
RSA	Redstone Arsenal
RWS	Roller Wheel Segmenting
TiAlN	Titanium Aluminum Nitride
TOW	Tube-Launched, Optically Tracked
WDI	Weapons Development and Integration
WJS	Water Jet Segmenting

REFERENCES

(1) **Jeffrey L. Lee and Jeffery S. Wright.** *Rocket Motor Segmenting.* April 2009, JANNAF.

(2) **www.efunda.com/materials/alloys/alloy_steels.** Alloy Steels. *eFunda.* [Online] [Cited: January 27, 2010.] www.efunda.com/materials/alloys/alloy_steels.

(3) **(ANSI), American National Standards Institute.** *Heat Treating of Steel Raw Materials.* Warrendale, PA: s.n., Reaffirmed, Apr 2006. AMS-H-6875.

(4) **E. Paul DeGarmo, J.T. Black, Ronald Kohser.** *Materials and Processes in Manufacturing.* 8th. New York: John Wiley & Sons, Inc., 1999.

(5) **Erik Oberg, Franklin D. Jones, Holbrook L. Horton, Henry H. Ryffel.** *Machinery's Handbook.* 28th. New York: Industrial Press, 2008.

(6) **Gradient Technology.** *M26 Multiple launch rocket system (MLRS) rocket motor segmenting using abrasive waterjet cutter.* Elk River, MN: Gradient Technology, 2008.

(7) **G. Sutter.** *Chip geometries during high-speed machining for othrogonal cutting conditions.* 57045 Metz Cedex 1, France: International Journal of Machine Tools & Manufacture, 2005, Vol. 45, pp. 719-726.

(8) **V.P. Astakhov, M.O.M. Osman, M.T. Hayajneh.** *Re-evaluation of the basic mechanics of orthogonal metal cutting: velocity diagram, virtual work equations and upper-bound theorem.* Montreal, Quebec: International Journal of Machine Tools & Manufacture, 2001, Vol. 41, pp. 393-418.

(9) **Tugrul Ozel.** *The influence of friction models on finite element simulations of machaning.* Piscataway, NJ: International Journal of Machine Tools & Manufacture, 2006, Vol. 46, pp. 518-530.

(10) **Mahmound Shatla, Christian Kerk, Taylan Altan.** *Process modeling in machaning. Part I: Determination of flow stress data.* Columbus, OH: International Journal of Machine Tools & Manufacture, 2001, Vol. 41, pp. 1551-1534.

(11) **Kuan-Ming Li, Steven Y. Liang.** *Modeling of cutting forces in near dry machining under tool wear effect.* Atlanta, GA: International Journal of Machine Tools & Manufacture, 2007, Vol. 47, pp. 1292-1301.

(12) **Marcio Bacci da Silva, James Wallbank.** *Cutting temperature: Prediction and measurement methods.* Coventry CV4 7AL, UK: Journal Materials Processing Technology, 1999, Vol. 88, pp. 195-202.

(13) **K.L. Johnson.** *Contact Mechanics.* Cambridge: Cambridge University Press, 1985.

(14) **Ansel C. Ugural, Saul K. Fenster.** *Advanced Strength and Applied Elasticity.* 4th. Upper Saddle River: Prentice Hall, 2003.

(15) **Avanish Kumar Dubey, Vino Yadava.** *Laser beam machining -A review.* Allahabad 211004, UP, India: International Journal of Machine Tools & Manufacture, 2008, Vol. 48, pp. 609-628.

(16) **N. Rajaram, J. Sheikh-Ahmad, S. H. Cheraghi.** *CO2 laser cut quality of 4130 steel.* Wichita, KS: International Journal of Machine Tools & Manufacture, 2003, Vol. 43, pp. 351-358.

(17) **Hongtao Ding, Yung C. Shin.** *Laser-assisted machining of hardened steel parts with surface integrity analysis.* West Lafayette, In: International Journal of Machine Tools & Manufacture, 2010, Vol. 50, pp. 106-114.

(18) **G. Bajinskis.** *Investigation of a propellant fire at Mulwala Explosives Factory.* 1985.

(19) **L.E. Jensen, K. R. Braegger, R.D. Glenn, J. A. Cox, W. D. Bolton.** *Solid propellant rocket motor dissection facility.* Brigham City, UT: JANNAF (1995), 1989. Vols. F04704-88-C-0015, pp. 121-130.

(20) **P. Kwon, T. Schiemann, R. Koutanya.** *An inverse estimation scheme to measure steady-state tool-chip interface temperatures using an infrared camera.* East Lansing, MI: International Journal of Machine Tools & Manufacture, 2001, Vol. 41, pp. 1015-1030.

(21) **Edward M. Trent, Paul K. Wright.** *Metal Cutting.* 4th. Boston: Butterworth Hinemann, 2000.

(22) **Yakup Yildoz, Maummer Nalbant.** *A review of cryogenic cooling in machining processes.* Ankara, Turkey: International Journal of Machine Tools & Manufacture, 2008, Vol. 48, pp. 947-964.